

Starting Off on the Wrong Foot: Pitfalls in Data Preparation

Jiayi Guo*

Panyi Dong[†]Zhiyu Quan[‡]

March 20, 2026

Abstract

When working with real-world insurance data, practitioners often encounter challenges during the data preparation stage that can undermine the statistical validity and reliability of downstream modeling. This study illustrates that conventional data preparation procedures such as random train-test partitioning, often yield unreliable and unstable results when confronted with highly imbalanced insurance loss data. To mitigate these limitations, we propose a novel data preparation framework leveraging two recent statistical advancements: support points for representative data splitting to ensure distributional consistency across partitions, and the Chatterjee correlation coefficient for initial, non-parametric feature screening to capture feature relevance and dependence structure. We further integrate these theoretical advances into a unified, efficient framework that also incorporates missing-data handling, and embed this framework within our custom InsurAutoML¹ pipeline. The performance of the proposed approach is evaluated using both simulated datasets and datasets often cited in the academic literature. Our findings definitively demonstrate that incorporating statistically rigorous data preparation methods not only significantly enhances model robustness and interpretability but also substantially reduces computational resource requirements across diverse insurance loss modeling tasks. This work provides a crucial methodological upgrade for achieving reliable results in high-stakes insurance applications.

Keyword: Data preparation; support point; Chatterjee correlation coefficient; missing data; AutoML; insurance data analytics; imbalance learning

*Actuarial and Risk Management Sciences, University of Illinois Urbana-Champaign, 1409 W. Green Street (MC-382), Urbana, IL 61801, USA. Email: jg54@illinois.edu.

[†]Actuarial and Risk Management Sciences, University of Illinois Urbana-Champaign, 1409 W. Green Street (MC-382), Urbana, IL, 61801, USA. Email: panyid2@illinois.edu.

[‡]Actuarial and Risk Management Sciences, University of Illinois Urbana-Champaign, 1409 W. Green Street (MC-382), Urbana, IL, 61801, USA. Email: zquan@illinois.edu.

¹<https://github.com/PanyiDong/InsurAutoML>.

1 Introduction

The well-known phrase “garbage in, garbage out,”² first recorded in 1957, remains highly relevant more than half a century later. Despite advances in statistical modeling and data science, the quality of input data continues to be a critical concern, particularly when working with real-world datasets. Even when data appear to be of reasonably high quality, practitioners often encounter numerous pitfalls during the data preparation phase that can undermine modeling efforts.

An initial step in the data science workflow is dividing the data into training and test sets. Common practices include k-fold cross-validation, leave-one-out cross-validation, and holdout methods. However, in actuarial modeling, the results of these conventional approaches are not always ideal. Insurance data are often highly imbalanced, for example, in loss modeling, the vast majority of policyholders may not file claims. A conventional approach that relies solely on a random train-test split can sow the seeds of failure in downstream actuarial modeling, leading to discrepancies in the proportion of zero claims or creating a distribution shift between the training and test datasets. Such imbalances can distort model evaluation and hinder model generalization, effectively leading the analysis to “start off on the wrong foot.”

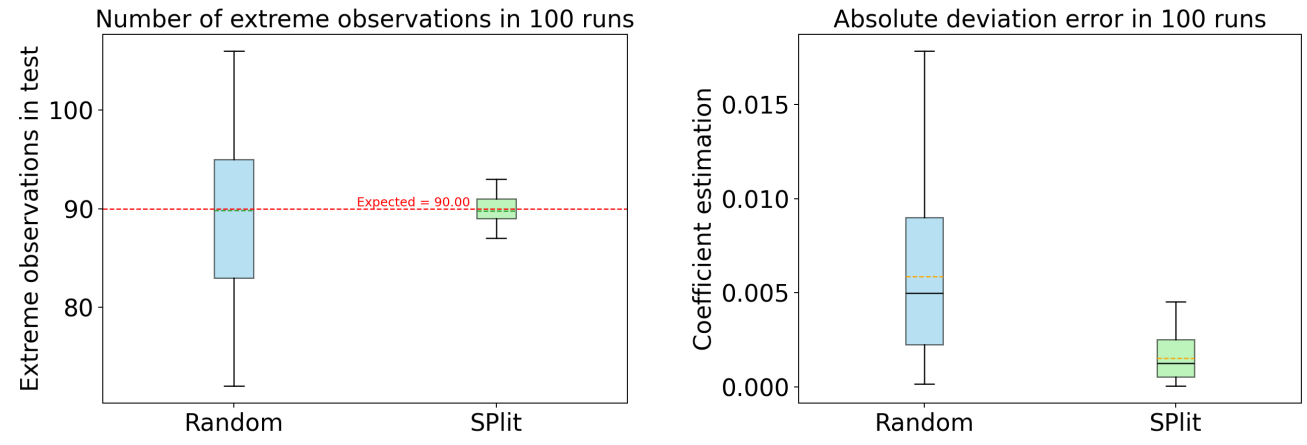
To illustrate, we conduct a controlled simulation based on a Tweedie mean–dispersion model with a single feature. Details of the Tweedie construction and simulation design are provided in Appendices B and C.1. Given this design, we examine two partitioning approaches: a conventional Random Splitting and *SPLIT*, a model-independent method for optimally dividing a dataset into training and test sets (Vakayil et al., 2022), which is discussed in detail in Section 2.1. *SPLIT* is designed to preserve distributional balance and can thus be directly contrasted with Random Splitting. Each method is applied at a 70/30 ratio, and both are evaluated on the same simulated datasets under matched random seeds, thereby isolating the effect of partitioning variation from the underlying data-generating process. To quantify these effects, we employ two complementary evaluation methods that assess how well each strategy preserves distributional properties.

Our first evaluation examines the representation of extreme observations (response variable) in test datasets. Specifically, we define a global threshold at the 97th percentile of the full Tweedie distribution, which is often considered a risky profile in insurance, and record the number of extreme observations allocated to the test set under each splitting strategy. To benchmark performance, the expected number of extreme observations in the test set is 90, given the 30% test proportion and our simulation setup. Figure 1(a) summarizes the number of extreme observations captured in the test set across 100 repeated experiments for both the Random Splitting and *SPLIT* methods. The Random Splitting yields an average of 89.86 number of extreme observations with a standard deviation of 7.72, whereas *SPLIT* yields an average of 89.77 with a substantially smaller standard deviation of 1.28. Both approaches can be considered as unbiased relative to the expected benchmark in repeated experiments, but *SPLIT* exhibits obviously greater stability by consistently allocating rare, extreme observations to the test set. Given

²Wikipedia, Garbage in, garbage out

that repeated real-world experiments are often computationally prohibitive, the stability offered by *SPLIT* highlights the importance of balance-preserving partitioning for reliable evaluation in heavy-tailed insurance contexts.

Our second evaluation assesses how accurately the regression coefficient is fitted under repeated data splits. For each training set, we fit a Tweedie regression model with the power parameter fixed at $q = 1.95$ (consistent with the simulation setup) and compute the absolute deviation between the estimated slope $\hat{\beta}$ and the true slope β_{true} (i.e., $|\hat{\beta} - \beta_{\text{true}}|$). Figure 1(b) reports the distribution of the absolute error across 100 repeated experiments for both splitting strategies. Under Random Splitting, the average error is 0.0059 with a standard deviation of 0.0044, relative to the true value $\beta_{\text{true}} = 0.2252$. In contrast, *SPLIT* reduces the average error to 0.0015 with a standard deviation of 0.0011. Although neither method shows systematic bias, errors of 2.6% for Random Splitting and 0.7% for *SPLIT*, the variance is substantially lower under *SPLIT*. This leads to more stable and reliable parameter estimation, particularly in settings with heavy-tailed or zero-inflated insurance datasets.



(a) Extreme observations captured (at 97th percentile threshold)

(b) Error distribution in coefficient estimation

Figure 1: Comparison between Random Splitting and *SPLIT* partitioning.

Overall, the findings highlight that the choice of data splitting method is crucial, even in controlled simulations without the additional noise present in real-world settings. Random Splitting, often utilized due to convenience in practice, can yield distorted test sets, particularly when dealing with imbalanced insurance datasets. In contrast, *SPLIT* preserves distributional balance and produces reproducible partitions, ensuring reliability for downstream modeling.

Another prevalent challenge in real-world insurance datasets is the “curse of dimensionality,” which is particularly pronounced in modern large-scale datasets. In contrast to the low-dimensional, curated data often found in academic examples, real-world data frequently comprises hundreds or even thousands of features. Discerning meaningful signals within such noisy and high-dimensional environments is a formidable task. Consequently, effective feature selection becomes crucial not only to reduce overfitting but also to retain signal and, figuratively

speaking, find the “needle in the haystack.” While recent studies attempt to address this, they remain largely model-dependent. For instance, Jeong (2022) combine categorical embeddings with principal component analysis (PCA) to reduce feature dimensionality while preserving critical risk information encoded in the data. Fung et al. (2023) propose a group-fused regularization approach to select statistically important features. Wang et al. (2023) develop a variable selection procedure within a Bayesian non-homogeneous hidden Markov model. Shi and Shi (2024) incorporate group lasso regularization to perform feature selection in the deep GLM model, a framework to capture frequency-severity distribution using deep neural networks. Liu et al. (2026) introduce Variational Automatic Relevance Determination (VARD) as a robust and efficient framework for variable selection and smoothness learning in additive models, where features can be precisely classified as having zero, linear, or nonlinear contribution to the response. However, a significant gap remains: these methods are often architecture-specific and lack the flexibility required for model-agnostic initial feature screening or universal application across complex non-linear structures.

Compounding these challenges is the pervasive issue of missing data. Unfortunately, improper handling remains widespread. Many practitioners resort to simplistic imputation methods, such as filling in missing values with the mean or median (simple imputation), or they exclude incomplete observations altogether (complete case analysis). These approaches ignore a rich body of research on principled methods for handling missing data, including multiple imputation and model-based techniques. While the availability of real-world insurance datasets has led to more specialized solutions, they remain largely context-specific. For example, Rosenberg et al. (2024) assume that data are “Not Missing At Random (NMAR)” and accordingly introduce a distinct category for missing values to capture responses such as “don’t know” or “refused.” Despite these individual advancements, a systematic and unified methodology for handling missingness remains elusive in the literature, particularly when these issues are intertwined with the data challenges mentioned earlier.

To address these often-overlooked data preparation challenges, we draw on practical insights from recent advances in theoretical statistics and adapt them to the actuarial context. Our work aims to develop tailored solutions for automatic, comprehensive, and informed data preparation in actuarial modeling, thereby enhancing the efficiency, robustness, and performance of previously proposed AutoML frameworks (Dong and Quan, 2025).

The remainder of the paper is structured as follows: Section 2 reviews the statistically informed data preparation methods. Section 3 proposes the informed data preparation pipelines and the integration of these pipelines with previously proposed AutoML frameworks. Section 4 illustrates the empirical performance of the proposed frameworks. Section 5 concludes. Please refer to Appendix A for the mathematical notations used in the paper.

2 Data Preparation Methodology

2.1 Data Splitting

Let $\mathcal{D} = \{\mathcal{O}_i = (\mathbf{X}_i, y_i)\}_{i=1}^N \in \mathbb{R}^{N \times (p+1)}$ be the dataset with N observations and each observation \mathcal{O}_i has p dimensional feature vector $\mathbf{X}_i = (X_{i1}, X_{i2}, \dots, X_{ip})$ and response y_i . Assume that \mathcal{O}_i is independently drawn from a distribution \mathcal{F} , i.e., $(\mathbf{X}_i, y_i) \stackrel{iid}{\sim} \mathcal{F} \quad i = 1, \dots, N$.

The aim is to fit a model $f(\mathbf{X}; \boldsymbol{\theta})$ to the data \mathcal{D} , where $\boldsymbol{\theta}$ is the unknown set of parameters in the model. In order to effectively learn the $\boldsymbol{\theta}$, we need to split data into $\mathcal{D}^{\text{train}}$ with size N_{train} and $\mathcal{D}^{\text{test}}$ with size N_{test} . Then the unknown parameters $\boldsymbol{\theta}$ are estimated by minimizing a loss function $\mathcal{L}(\mathbf{y}, f(\mathbf{X}; \boldsymbol{\theta}))$ on the $\mathcal{D}^{\text{train}}$, i.e.,

$$\hat{\boldsymbol{\theta}} = \underset{\boldsymbol{\theta}}{\operatorname{argmin}} \frac{1}{N_{\text{train}}} \sum_{i=1}^{N_{\text{train}}} \mathcal{L}(y_i^{\text{train}}, f(\mathbf{X}_i^{\text{train}}; \boldsymbol{\theta}))$$

Hopefully, the trained predictive model $f(\mathbf{X}; \hat{\boldsymbol{\theta}})$ is close to the true model $E(\mathbf{y}|\mathbf{X})$. To quantify the model performance, define the generalization error as

$$\varepsilon = E_{\mathbf{X}, \mathbf{y}} \left\{ \mathcal{L}(\mathbf{y}, f(\mathbf{X}; \hat{\boldsymbol{\theta}})) \mid D \right\}$$

where $\hat{\boldsymbol{\theta}}$ is the estimate of $\boldsymbol{\theta}$ from $\mathcal{D}^{\text{train}}$ and the expectation is taken with respect to a realization (\mathbf{X}, \mathbf{y}) from \mathcal{F} .

An estimate of the generalization error, ε , can be obtained from the test set as

$$\hat{\varepsilon} = \frac{1}{N_{\text{test}}} \sum_{j=1}^{N_{\text{test}}} \mathcal{L}(y_j^{\text{test}}, f(\mathbf{X}_j^{\text{test}}; \hat{\boldsymbol{\theta}}))$$

and we denote $\mathcal{T}_j = (\mathbf{X}_j^{\text{test}}, y_j^{\text{test}})$ as the j th observation in $\mathcal{D}^{\text{test}}$. The estimate of the generalization error is unbiased if $\mathcal{T}_j \sim \mathcal{F}$, $j = 1, \dots, N_{\text{test}}$.

Random sampling is the easiest method to ensure unbiased conditions, which requires that the test observation follows the true distribution. Then, $\hat{\varepsilon}$ can be viewed as the Monte Carlo (MC) estimate of ε . However, random sampling gives a high error rate of $O\left(N_{\text{test}}^{-\frac{1}{2}}\right)$ for $|\hat{\varepsilon} - \varepsilon|$, whereas when sampling from uniform distributions, quasi-Monte Carlo (QMC) error rate can be shown to be almost $O\left(N_{\text{test}}^{-1}\right)$ (Niederreiter, 1992). This consideration is particularly critical in actuarial modeling, where slow convergence in the model's error rate can lead to significant issues, as discussed in the Introduction. Unlike experimental or academic settings where extensive computational resources may be available to run numerous replications, real-world actuarial applications often operate under practical constraints. Limited computational budgets, whether due to time, cost, or infrastructure, may only allow for a single or a few iterations of data splitting and model training. As a result, the choice of data partitioning strategy and its stability

becomes especially consequential. As Höfling and Tibshirani (2008) demonstrate, when data are limited, the way observations are partitioned into training and test sets can affect both the accuracy of the fitted model and the reliability of performance evaluation. An unreliable or unrepresentative train-test split can yield misleading estimates of model performance, leading to suboptimal decision-making in high-stakes insurance applications. Therefore, understanding and mitigating the implications of error rate variability under restricted computational settings is essential for reliable and responsible actuarial modeling.

To get a more efficient sampling, Mak and Joseph (2018) propose the support points to obtain a QMC sample from general distributions which guarantee a convergence rate faster than MC (e.g., random sampling) by $\log(N_{\text{test}})$ factor, i.e., $|\hat{\varepsilon} - \varepsilon| \leq C\sqrt{\overline{\mathbb{E}\mathbb{D}}}$ where C is a constant that does not depend on the test sample, and $\overline{\mathbb{E}\mathbb{D}}$ is the energy distance between the test sample and the distribution \mathcal{F} . The energy distance can be estimated from the data using

$$\overline{\mathbb{E}\mathbb{D}}_{N_{\text{test}},N} = \frac{2}{N_{\text{test}}N} \sum_{j=1}^{N_{\text{test}}} \sum_{i=1}^N \|\mathcal{T}_j - \mathcal{O}_i\|_2 - \frac{1}{N_{\text{test}}^2} \sum_{j=1}^{N_{\text{test}}} \sum_{j'=1}^{N_{\text{test}}} \|\mathcal{T}_j - \mathcal{T}_{j'}\|_2 - \frac{1}{N^2} \sum_{i=1}^N \sum_{i'=1}^N \|\mathcal{O}_i - \mathcal{O}_{i'}\|_2$$

where $\|\cdot\|_2$ is the ℓ_2 norm. Since the energy distance does not depend on the model $f(\cdot; \boldsymbol{\theta})$ nor the loss function $\mathcal{L}(\cdot, \cdot)$, a model-independent test set can be obtained by minimizing the energy distance. Intuitively, minimizing the energy distance involves considering its three main components. The first component requires minimizing the Euclidean distance between observations from the underlying dataset and those from the test dataset, thereby encouraging similarity between the two distributions. In contrast, the second and third components involve maximizing the within-group Euclidean distances, e.g., among observations within the test set. This promotes a broader spread or dispersion of samples within each group, helping to avoid clustering and ensuring better representation of the underlying distribution. Together, these objectives contribute to a more balanced and representative data split.

The minimizer of the energy distance is referred to as support points (Mak and Joseph, 2018):

$$\{\boldsymbol{o}_j^*\}_{j=1}^{N_{\text{test}}} = \arg \min_{\{\boldsymbol{o}_j\}_{j=1}^{N_{\text{test}}}} \overline{\mathbb{E}\mathbb{D}}_{N_{\text{test}},N} = \arg \min_{\{\boldsymbol{o}_j\}_{j=1}^{N_{\text{test}}}} \frac{2}{N_{\text{test}}} \sum_{j=1}^{N_{\text{test}}} \mathbb{E} \|\boldsymbol{o}_j - \boldsymbol{\mathcal{O}}\|_2 - \frac{1}{N_{\text{test}}^2} \sum_{j=1}^{N_{\text{test}}} \sum_{j'=1}^{N_{\text{test}}} \|\boldsymbol{o}_j - \boldsymbol{o}_{j'}\|_2 \quad (2.1)$$

Support points, \boldsymbol{o}_j^* , can be viewed as the representative points of the distribution \mathcal{F} , which is the best set of N_{test} points to represent \mathcal{F} according to the energy distance criterion. Support points converge in distribution to \mathcal{F} and therefore, they can be viewed as a QMC sample from \mathcal{F} .

However, in the real-world, we rarely know the distribution \mathcal{F} , instead, we only have a dataset \mathcal{D} , which is assumed to be a set of independent realizations from \mathcal{F} . Hence, we are only able to compute the support points empirically, by replacing the expectation in Equation 2.1 with the MC average computed over \mathcal{D}

$$\{\mathbf{o}_j^*\}_{j=1}^{N_{\text{test}}} = \arg \min_{\{\mathbf{o}_j\}_{j=1}^{N_{\text{test}}}} \frac{2}{N_{\text{test}}N} \sum_{j=1}^{N_{\text{test}}} \sum_{i=1}^N \|\mathbf{o}_j - \mathbf{o}_i\|_2 - \frac{1}{N_{\text{test}}^2} \sum_{j=1}^{N_{\text{test}}} \sum_{j'=1}^{N_{\text{test}}} \|\mathbf{o}_j - \mathbf{o}_{j'}\|_2$$

This empirical estimation is implemented in the R package *support*³ and *SPLIT*⁴, and we incorporate this into our Python AutoML framework (Dong and Quan, 2025). Support points give the best possible representation of the dataset \mathcal{D} , according to the energy distance criterion, and therefore, the data splitting algorithm is expected to produce a test set that is best for evaluating the performance of a model fitted on the training set.

In addition, k-fold cross-validation is frequently employed to obtain more robust estimates of model performance in practice. Standard k-fold cross-validation typically relies on random partitioning of the data, which can still introduce some of the issues highlighted in the Introduction. However, the impact of random partitioning is somewhat mitigated in this setting because the generalization error is estimated by aggregating error measures across all k folds. As a result, the variability due to any single split is averaged out, yielding a more stable error estimate. Nevertheless, the reliability of cross-validation still depends on how well each fold reflects the overall data distribution. If the folds are not representative, bias in performance evaluation may persist. This observation highlights that principled data splitting strategies, such as those based on minimizing energy distance, remain relevant and beneficial even within k-fold cross-validation frameworks. To further accelerate and improve the computation efficiency of the proper data partitioning, Vakayil and Joseph (2022) propose the *Data Twinning*⁵ algorithm, which is theoretically related to *SPLIT* but incorporates numerical optimization techniques to achieve more efficient data splitting. In addition, empirically, cross-validation based on *Data Twinning* has been shown to require fewer folds than cross-validation with Random Splitting. This empirical evidence offers a significant computational advantage, particularly when tuning models that are computationally expensive to train. By reducing the number of folds needed for reliable error estimation, *Data Twinning* not only accelerates the cross-validation process but also helps offset the computational cost associated with implementing more principled data-splitting methods.

2.2 Feature Selection

In real-world data science applications, it is often unclear whether the collected features are truly relevant to the response variable. A common preliminary step in feature selection, particularly in the context of ordinary linear regression, is to compute Pearson’s correlation coefficient. Since Pearson’s coefficient is directly related to the linear model coefficient, it provides a straightforward measure of linear association between features and the response variable. However, its utility is limited to detecting strictly linear relationships. Alternative measures such as Spearman’s rank correlation or Kendall’s tau extend the analysis to monotonic associations, yet they too fail to capture more complex, non-monotonic associations, even in the absence of

³<https://CRAN.R-project.org/package=support>

⁴<https://CRAN.R-project.org/package=SPLIT>

⁵<https://CRAN.R-project.org/package=twinning> <https://github.com/avkl/twinning>

noise. Consequently, these traditional correlation coefficients are of limited value in practice, where relationships among variables rarely conform to simple linear or monotonic structures. To address these limitations, Chatterjee (2021) propose a novel correlation coefficient designed as a consistent estimator of a general measure of dependence. This coefficient, following Rényi’s criteria, equals zero if and only if the variables are independent, and equals one if and only if one variable is a measurable function of the other.

Formally, the Chatterjee Correlation Coefficient (CCC) (Chatterjee, 2021) for the univariate case (\mathbf{X}, \mathbf{y}) with $p = 1$ is defined as

$$CCC_N(\mathbf{X}, \mathbf{y}) = 1 - \frac{N \sum_{i=1}^{N-1} |r_{i+1} - r_i|}{2 \sum_{i=1}^N l_i(N - l_i)}.$$

To compute this, the dataset \mathcal{D} is first ordered by the feature \mathbf{X} , i.e., $X_{[1]} \leq \dots \leq X_{[N]}$, yielding the rearranged pairs $\mathcal{D} = \{(X_{[i]}, y_{[i]})\}_{i=1}^N$. Here, r_i be the number of j such that $y_{[j]} \leq y_{[i]}$, i.e., $r_i = \sum_{j=1}^N \mathbb{1}_{y_{[j]} \leq y_{[i]}}$, and similarly, l_i be the number of j such that $y_{[j]} \geq y_{[i]}$, i.e., $l_i = \sum_{j=1}^N \mathbb{1}_{y_{[j]} \geq y_{[i]}}$.

In the absence of ties among the y_i , l_1, \dots, l_N is simply a permutation of $1, \dots, N$, and the formula reduces to the simplified form

$$CCC_N(\mathbf{X}, \mathbf{y}) = 1 - \frac{N \sum_{i=1}^{N-1} |r_{i+1} - r_i|}{N(N^2 - 1)/3} = 1 - \frac{3}{N^2 - 1} \sum_{i=1}^{N-1} |r_{i+1} - r_i|.$$

Importantly, CCC retains the desirable property of having a tractable asymptotic distribution under the null hypothesis of independence, analogous to traditional correlation measures. This property makes it particularly appealing for statistical inference and offers a stronger foundation for feature screening in high-dimensional and noisy real-world datasets (Shi et al., 2021). For example, CCC does not require any restrictions on the distribution of \mathbf{X} and \mathbf{y} other than that \mathbf{y} is not a constant. \mathbf{X} and \mathbf{y} can be discrete, continuous, light-tailed, or heavy-tailed. CCC remains unchanged if we apply strictly increasing transformations to \mathbf{X} and \mathbf{y} , since its calculation is based on ranks. That said, CCC is inherently restricted to the univariate feature setting. In practice, however, most real-world datasets involve multiple features ($p > 1$), where a multivariate extension is needed.

To address this, Azadkia and Chatterjee (2021) introduce the Azadkia-Chatterjee correlation coefficient (ACCC), defined as

$$ACCC_N(\mathbf{X}, \mathbf{y}) = \frac{\sum_{i=1}^N (N \times \min(r_i, r_{NN(i)}) - l_i^2)}{\sum_{i=1}^N l_i(N - l_i)},$$

where $NN(i)$ denotes the index j such that \mathbf{X}_j is the nearest neighbor of \mathbf{X}_i , and $r_i = \sum_{j=1}^N \mathbb{1}_{y_j \leq y_i}$, $l_i = \sum_{j=1}^N \mathbb{1}_{y_j \geq y_i}$.

If there are no ties among the y_i , the expression further simplifies to

$$ACCC_N(\mathbf{X}, \mathbf{y}) = \frac{\sum_{i=1}^N \min(r_i, r_{NN(i)}) - (N + 1)(2N + 1)/6}{(N^2 - 1)/6}.$$

Together, CCC and ACCC provide a modern toolkit for dependence measurement, extending beyond the limitations of traditional correlation coefficients by consistently detecting both linear and nonlinear associations. Although CCC and ACCC provide distribution- and model-free measures of dependence, both estimators rely on the ranking (or nearest neighbors) of \mathbf{X} or \mathbf{y} . For example, in CCC, $r_i = \sum_{j=1}^N \mathbb{1}_{\{y_{[j]} \leq y_{[i]}\}}$ relies on the rearranged feature values $\{X_{[i]}\}_{i=1}^N$, while ACCC depends on nearest neighbors in the L^2 space. This dependence raises practical challenges in the presence of ties in rankings or distances. For continuously distributed variables, ties are rare and the induced order is usually trivial. However, ties frequently arise for categorical variables and compound distributions, such as the Tweedie distribution, which is commonly used in insurance modeling. In particular, insurance claim data often exhibit excessive zeros and extreme skewness; in commercial or catastrophe insurance, zeros may comprise up to 99% of observations, making ties in rankings or nearest neighbors almost unavoidable. In such settings, ties occur frequently and can materially affect correlation estimation⁶. Although CCC and ACCC theoretically converge regardless of distributional assumptions, in practice, the presence of ties still introduces ambiguity for empirical estimation. The original methods address this issue through tie-breaking strategies: random tie-breaking for duplicate values in univariate \mathbf{X} for CCC or equidistant nearest neighbors for ACCC, and maximal or ordinal tie-breaking for ties in \mathbf{y} (i.e., assign the maximum of the ranks that would have been assigned to all the tied values). However, random tie-breaking introduces additional variability into the estimated correlations. In datasets with many ties, this variability can substantially affect the estimated correlations, thereby influencing the outcomes of feature selection. As illustrated in Appendix F, different tie-breaking strategies can lead to noticeable variation in estimated correlations for features with ties, and in extreme cases may result in different features being selected. To mitigate this issue, prior work recommends repeating the estimation multiple times and averaging the results to improve stability. An alternative approach is to add zero-mean, extremely small-variance noise to tied features to break ties implicitly and average estimates across multiple noise realizations, thereby yielding similar stabilizing effects without artificial tie-breaking rules. In our experiments, estimates are computed using 20 independent repetitions with random tie-breaking for \mathbf{X} and ordinal tie-breaking for \mathbf{y} (i.e., preserving the order of appearance in the dataset). The final correlation estimate is obtained by averaging across these repetitions. A detailed discussion of tie-breaking strategies and their impact on CCC and ACCC is provided in Appendix F.

2.3 Missing Data

According to the classical framework established by Rubin (1976) and further developed by Rubin and Little (1987), missing data mechanisms can be categorized into three types: (a) *Missing Completely at Random* (MCAR): Under the MCAR mechanism, the missingness is entirely unrelated to both the observed and unseen components of the dataset. In other words, the occurrence of missingness is purely random, and the missing values do not depend on any

⁶These limitations are not unique to CCC and ACCC; other conventional correlation estimators also face significant challenges when applied to insurance data.

variable in the data. Consequently, the distribution of the observed data is not systematically different from the distribution of the missing data. Although this assumption is convenient, since many traditional statistical methods yield unbiased results under MCAR, it is rarely satisfied in real-world applications, where missingness typically exhibits some structure. (b) *Missing at Random* (MAR): The MAR mechanism, sometimes called conditionally missing at random, posits that missingness depends on the observed parts but not the unseen values. That is, after conditioning on the available information, the probability of missingness is independent of the missing values. MAR is a more realistic assumption in practice than MCAR and serves as the foundation for many modern techniques of handling missing data, such as multiple imputation and likelihood-based approaches. (c) *Missing Not at Random* (MNAR). In contrast, under the MNAR mechanism or not missing at random (alternative naming), the probability of missingness is directly related to the unseen values themselves. In this case, the data of interest differ systematically between observed and missing observations, even after conditioning on all available information. Because the missingness mechanism depends on unobserved data, MNAR is the most difficult case to address and often requires explicit modeling of the missing data process or strong external assumptions. Gomer and Yuan (2021) further subdivide the MNAR mechanism into two subtypes. *Focused MNAR* refers to situations where a variable governs its own missingness, i.e., the probability of being missing depends directly on the value of that same variable. In contrast, *Diffuse MNAR* arises when the missingness of one variable is driven by the values of other unobserved variables in the dataset.

We discuss missing data mechanisms because the choice of analytical method for handling missingness can critically affect the validity of subsequent analyses. Certain approaches, while convenient rule of thumb as described in Figure 1 in the survey paper (Mirzaei et al., 2022), are theoretically problematic and may introduce bias. In particular, naive but commonly used strategies, such as Complete Case Analysis (discarding all observations with missing values) or Simple Imputation methods (replacing missing values with the mean, median, or other basic statistics), can yield biased results under both MAR and MNAR mechanisms. In Section 4, we demonstrate how missing data can distort inference and compromise the reliability of downstream analyses.

The challenge of handling missing data has been studied extensively across disciplines, as failure to properly address it can compromise statistical analyses and lead to biased or incorrect conclusions. For the sake of brevity, we group existing approaches into three broad categories: statistical approaches based on certain assumptions, non-parametric approaches leveraging machine learning, and emerging approaches employing modern computational techniques.

For the statistical approach, one of the earliest and most widely used methods is maximum likelihood estimation (MLE), which dates back to the 1950s (Lord, 1955). The classical MLE uses iterative optimization to estimate model parameters that minimize the sum of squared standardized distances between a model’s predictions and the observed data. The log-likelihood formulation assumes that all participants share the same model parameters, but each observation’s contribution to estimation is restricted to the subset of parameters for which data are available. Although MLE does not directly impute missing values, the multivariate normal log-likelihood effectively acts as an imputation technique: it leverages the observed data to

infer the likely location of missing points and adjusts model parameters accordingly. Traditional approaches typically assume a joint distribution for incomplete variables, most often the multivariate normal. By contrast, factored regression (Lüdtke et al., 2020) acknowledges the existence of a multivariate distribution without requiring researchers to fully specify its form. Instead, it applies the probability chain rule to factorize the joint distribution into a sequence of univariate conditional distributions, each corresponding to a regression model.

Among non-parametric approaches, imputation-based techniques are frequently employed to replace missing values with predicted values derived from the observed portion of the dataset, without imposing certain assumptions as in statistical approaches. Generally, single imputation methods, including the previously mentioned Simple Imputation, are computationally simple but statistically problematic, as they ignore uncertainty associated with missing and tend to produce biased estimates. To address this, multiple imputation (MI) (Rubin, 2018) has become a standard method under the MAR assumption. MI generates several plausible imputed datasets by imitating the distribution of observed data, fits the desired model to each dataset, and then combines estimates to produce a valid inference that reflects uncertainty about the missing values. Popular implementations include Fully Conditional Specification (FCS), operationalized through the Multiple Imputation by Chained Equations (MICE) algorithm (Van Buuren and Groothuis-Oudshoorn, 2011), and MissForest, an iterative non-parametric imputation method based on random forests (Stekhoven and Bühlmann, 2012) and similar tree-based methods have been demonstrated by Loh et al. (2019) to offer robust, practical alternatives for reliably handling incomplete data. Both methods have been shown to perform well empirically in high-dimensional and nonlinear settings.

Lastly, we point out some emerging approaches based on recent techniques. For instance, Gan and Yan (2025) extend and explore an imputation method based on generative adversarial networks (GANs) to impute missing values in insurance data, demonstrating the potential of deep learning methods. A recent paper by Mohan and Pearl (2021) argue that graphical models provide a principled framework for reasoning about missingness mechanisms. By representing dependencies between variables explicitly, graphical models can identify testable conditional independence relations and determine whether a parameter of interest is recoverable from incomplete data (i.e., whether a consistent estimator exists for a given mechanism). These developments open promising directions for actuarial science, where translating theoretical advances into practical tools remains an important area of future research.

In real-world applications, it is generally impossible to distinguish between MAR and MNAR mechanisms using observed data alone (Little, 1993). Siddique et al. (2012) further show that uncertainty about the missing-data mechanism can substantially affect post-imputation inference. As a result, practitioners must often rely on subject-matter expertise and conduct sensitivity analyses to evaluate the robustness of their findings under alternative assumptions. Efromovich (2017) comprehensively discuss different types of missing mechanisms and suggest how they should be treated in non-parametric regression tasks in actuarial science. Moreover, imputation becomes increasingly difficult as the number of variables grows, due to the curse of dimensionality. This difficulty is consistent with the broader statistical literature, where Loh and Wainwright (2011) show that high-dimensional regression with noisy and missing covariates

require dedicated estimators with provable statistical guarantees and computationally efficient algorithms. Computational efficiency therefore becomes another important concern: advanced imputation methods, while powerful, may be computationally demanding, making scalable and efficient implementations essential for large actuarial datasets.

3 Informed Data Preparation

3.1 Informed Data Preparation Pipeline

We propose two statistically informed data preparation pipelines (IDPP) by integrating the data preparation methods discussed in Section 2 to address common challenges in real-world data, including missing values, redundant or irrelevant features, and more informative train–test splitting. By leveraging domain-informed statistical tools, the IDPP outperform approaches that randomly combine data preprocessing steps, such as the pipeline in Dong and Quan (2025), where the choice of encoding, imputation, balancing, scaling, and feature selection methods is considered as the hyperparameter and randomly sampled from the hyperparameter search space to optimize downstream performance. Given the input dataset $\mathcal{D}^{input} = (\mathbf{X}, \mathbf{y}) = \{\mathcal{O}_i = (\mathbf{X}_i, y_i)\}_{i=1}^N \in \mathbb{R}^{N \times (p+1)}$, the first preparation pipeline, \mathcal{IDPP}^{comp} , samples and processes only completely observed instances (i.e., without missing values). The second pipeline, \mathcal{IDPP}^{miss} , is designed to preprocess datasets that contain missing values. Figure 2 illustrates the two informed data preparation pipelines using a simple example.

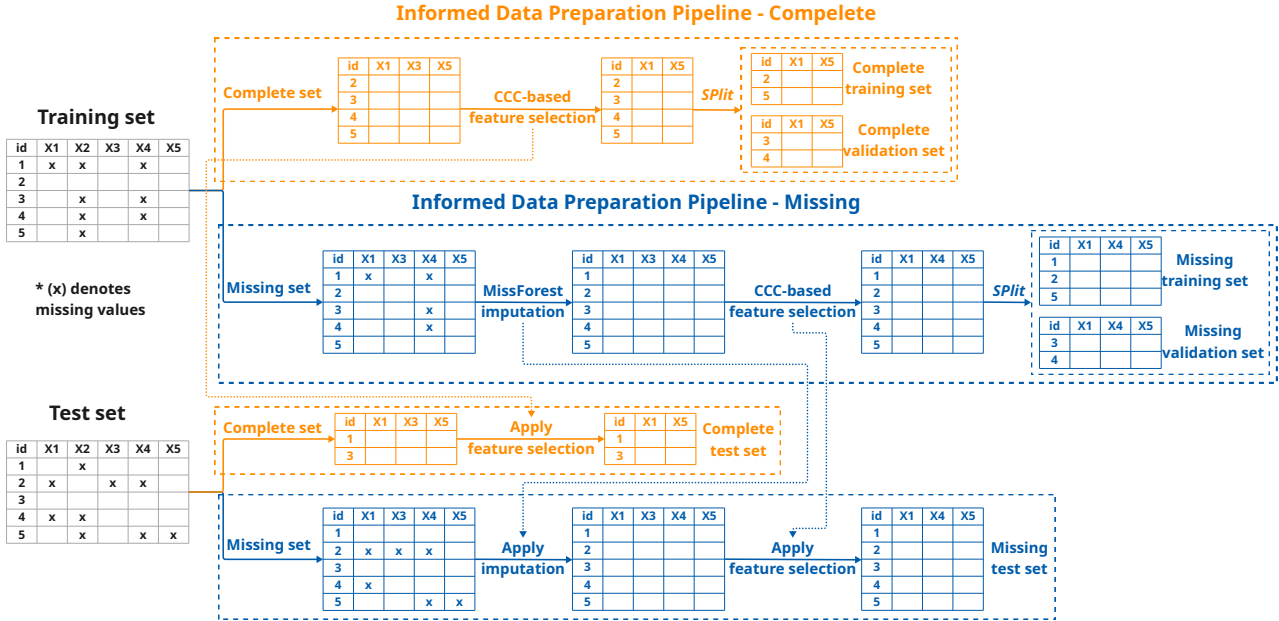


Figure 2: An illustration of the Informed Data Preparation Pipeline

For the complete preparation pipeline, \mathcal{IDPP}^{comp} , the pipeline selects the non-missing

data from the input dataset by performing two steps. First, we delete features with a significant portion of missing data. We calculate each feature's missing rate, i.e., j -th feature with missing rates $R_j = \frac{1}{N} \sum_{i=1}^N \mathbb{1}_{\{X_{ij} \text{ is missing}\}}$, $j = 1, 2, \dots, p$. Then, we delete the features whose missing rates, R_j , exceed certain pre-defined missing threshold λ_{miss}^{comp} , by generating a matrix $\mathbf{W}^{comp,comp} \in \{0, 1\}^{p \times p_{comp}^{comp}}$. Here, $p_{comp}^{comp} = \sum_{j=1}^p \mathbb{1}_{\{R_j \leq \lambda_{miss}^{comp}\}}$ denotes the number of selected features after the first step. For $\mathbf{W}^{comp,comp}$, each element satisfies $W_{j, \sum_{i=1}^j \mathbb{1}_{\{R_i \leq \lambda_{miss}^{comp}\}}}^{comp,comp} = \mathbb{1}_{\{R_j \leq \lambda_{miss}^{comp}\}}$, $j = 1, \dots, p$, and equals 0 otherwise. Second, we further delete observations (rows) with missing values. Then the complete set is defined as

$$\mathcal{D}^{comp} = \{(\mathbf{X}_i \mathbf{W}^{comp,comp}, y_i) : (\mathbf{X}_i, y_i) \in \mathcal{D}^{input}, \mathbf{X}_i \mathbf{W}^{comp,comp} \text{ has no missing value}\}.$$

We denote the size of this complete set as $N^{comp} = |\mathcal{D}^{comp}|$ ($\mathcal{D}^{comp} \in \mathbb{R}^{N^{comp} \times (p_{comp}^{comp} + 1)}$). Once the complete data is selected, we perform CCC-based feature selection to screen informative features. Specifically, by setting a CCC feature selection threshold λ_{CCC}^{comp} , the element of CCC feature selection matrix $\mathbf{W}^{comp,CCC} \in \{0, 1\}^{p_{comp}^{comp} \times p_{CCC}^{comp}}$ (p_{CCC}^{comp} denotes number of complete features selected by CCC) satisfies $W_{j, \sum_{i=1}^j \mathbb{1}_{\{CCC_{N^{comp}}(\mathbf{x}^i, \mathbf{y}) \geq \lambda_{CCC}^{comp}\}}}^{comp,CCC} = \mathbb{1}_{\{CCC_{N^{comp}}(\mathbf{x}^j, \mathbf{y}) \geq \lambda_{CCC}^{comp}\}}$, $j = 1, 2, \dots, p_{comp}^{comp}$, where $\mathbf{X}^j = (X_{1j}, X_{2j}, \dots, X_{N^{comp}j})^T$, $j = 1, 2, \dots, p_{comp}^{comp}$, refers the j -th feature vector, and equals 0 otherwise. Thus, this generates a complete set selected by CCC feature selection,

$$\mathcal{D}_{CCC}^{comp} = \{(\mathbf{X}_i \mathbf{W}^{comp,CCC}, y_i) : (\mathbf{X}_i, y_i) \in \mathcal{D}^{comp}\} \in \mathbb{R}^{N^{comp} \times (p_{CCC}^{comp} + 1)}.$$

In practice, one may set the top number/percentage of features selected by CCC, instead of the feature selection threshold λ_{CCC}^{comp} to prevent extreme over/under selection. The *SPLIT* is then applied to get the complete validation set

$$\mathcal{D}_{valid}^{comp} = \{\mathbf{o}_j \in \mathcal{D}_{CCC}^{comp} : \mathbf{o}_j \text{ is a support point of } \mathcal{D}_{CCC}^{comp}\} \in \mathbb{R}^{N_{valid}^{comp} \times (p_{CCC}^{comp} + 1)}$$

and complete training set $\mathcal{D}_{train}^{comp} = \mathcal{D}_{CCC}^{comp} \setminus \mathcal{D}_{valid}^{comp} \in \mathbb{R}^{N_{train}^{comp} \times (p_{CCC}^{comp} + 1)}$, ($N_{train}^{comp} = N^{comp} - N_{valid}^{comp}$), where $N_{valid}^{comp} = |\mathcal{D}_{valid}^{comp}|$ is the number of complete validation set. For the purpose of evaluating model generalizability, we perform the same feature selection procedure and complete-case selection on the test set to ensure consistency. Algorithm 1 summarizes \mathcal{IDPP}^{comp} .

For the missing preparation pipeline, \mathcal{IDPP}^{miss} , instead of sampling over both observations and features, the pipeline selects features based on a missing threshold from the input dataset

$$\mathcal{D}^{miss} = (\mathbf{X} \mathbf{W}^{miss,miss}, \mathbf{y}) \in \mathbb{R}^{N \times (p_{miss}^{miss} + 1)}$$

by defining missing feature selection matrix $\mathbf{W}^{miss,miss}$ using pre-defined missing threshold λ_{miss}^{miss} and selecting p_{miss}^{miss} number of missing features. It should be noted that different from complete set where \mathcal{D}^{comp} contains no missing values, missing set \mathcal{D}^{miss} includes missing values and is therefore not directly suitable for modeling; however we can preserve more data from the original input dataset. An imputation procedure, specifically MissForest (Stekhoven and Bühlmann, 2012) in this work, is applied to obtain an imputed dataset $\mathcal{D}_{imputed}^{miss} \in \mathbb{R}^{N \times (p_{miss}^{miss} + 1)}$. To ensure consistency, we utilize a MissForest implementation that reuses the tree models trained on

Algorithm 1: The Complete Informed Data Preparation Pipeline $IDPP^{comp}$

Input: Input Dataset \mathcal{D}^{input} ; Missing threshold λ_{miss}^{comp} ; CCC feature selection threshold λ_{CCC}^{comp}

Output: Complete training set $\mathcal{D}_{train}^{comp}$; Complete validation set $\mathcal{D}_{valid}^{comp}$

- 1 Compute matrix $\mathbf{W}^{comp,comp}$ based on λ_{miss}^{comp} ;
- 2 $\mathcal{D}^{comp} = \{(\mathbf{X}_i \mathbf{W}^{comp,comp}, y_i) : (\mathbf{X}_i, y_i) \in \mathcal{D}^{input}, \mathbf{X}_i \mathbf{W}^{comp,comp} \text{ has no missing value}\}$;
/* Complete-case selection */
- 3 Compute CCC feature selection matrix $\mathbf{W}^{comp,CCC}$ based on λ_{CCC}^{comp} ;
- 4 $\mathcal{D}_{CCC}^{comp} = \{(\mathbf{X}_i \mathbf{W}^{comp,CCC}, y_i) : (\mathbf{X}_i, y_i) \in \mathcal{D}^{comp}\}$; /* CCC feature selection */
- 5 $\mathcal{D}_{valid}^{comp} = \{\mathbf{o}_j \in \mathcal{D}_{CCC}^{comp} : \mathbf{o}_j \text{ is a support point of } \mathcal{D}_{CCC}^{comp}\}$;
- 6 $\mathcal{D}_{train}^{comp} = \mathcal{D}_{CCC}^{comp} \setminus \mathcal{D}_{valid}^{comp}$; /* Split */
- 7 **return** $\mathcal{D}_{train}^{comp}, \mathcal{D}_{valid}^{comp}$;

the training set to impute missing values in the validation and test datasets. Following the imputation, we apply the CCC-based feature selection on the imputed set

$$\mathcal{D}_{CCC}^{miss} = \{(\mathbf{X}_i \mathbf{W}^{miss,CCC}, y_i) : (\mathbf{X}_i, y_i) \in \mathcal{D}_{imputed}^{miss}\} \in \mathbb{R}^{N \times (p_{CCC}^{miss} + 1)}$$

where $\mathbf{W}^{miss,CCC}$ denotes the CCC feature selection matrix and p_{CCC}^{miss} represents the number of features selected by CCC in the missing preparation pipeline, defined analogously to their counterparts in the complete preparation pipeline. The missing validation set is then defined as

$$\mathcal{D}_{valid}^{miss} = \{\mathbf{o}_j \in \mathcal{D}_{CCC}^{miss} : \mathbf{o}_j \text{ is a support point of } \mathcal{D}_{CCC}^{miss}\} \in \mathbb{R}^{N_{valid}^{miss} \times (p_{CCC}^{miss} + 1)}$$

with N_{valid}^{miss} as the size of the missing validation set. The missing training set is $\mathcal{D}_{train}^{miss} = \mathcal{D}_{CCC}^{miss} \setminus \mathcal{D}_{valid}^{miss} \in \mathbb{R}^{N_{train}^{miss} \times (p_{CCC}^{miss} + 1)}$ ($N_{train}^{miss} = N - N_{valid}^{miss}$). For the purpose of evaluating model generalizability, we perform the same feature selection procedures and MissForest imputation on the test set to ensure consistency. Algorithm 2 summarizes $IDPP^{miss}$.

Algorithm 2: The Missing Informed Data Preparation Pipeline $IDPP^{miss}$

Input: Input Dataset \mathcal{D}^{input} ; Missing threshold λ_{miss}^{miss} ; CCC feature selection threshold λ_{CCC}^{miss}

Output: Missing training set $\mathcal{D}_{train}^{miss}$; Missing validation set $\mathcal{D}_{valid}^{miss}$

- 1 Compute matrix $\mathbf{W}^{miss,miss}$ based on λ_{miss}^{miss} ;
- 2 $\mathcal{D}^{miss} = (\mathbf{X} \mathbf{W}^{miss,miss}, \mathbf{y})$; /* Missing-case feature selection */
- 3 Get imputed set $\mathcal{D}_{imputed}^{miss}$; /* MissForest imputation */
- 4 Compute CCC feature selection matrix $\mathbf{W}^{miss,CCC}$ based on λ_{CCC}^{miss} ;
- 5 $\mathcal{D}_{CCC}^{miss} = \{(\mathbf{X}_i \mathbf{W}^{miss,CCC}, y_i) : (\mathbf{X}_i, y_i) \in \mathcal{D}_{imputed}^{miss}\}$; /* CCC feature selection */
- 6 $\mathcal{D}_{valid}^{miss} = \{\mathbf{o}_j \in \mathcal{D}_{CCC}^{miss} : \mathbf{o}_j \text{ is a support point of } \mathcal{D}_{CCC}^{miss}\}$;
- 7 $\mathcal{D}_{train}^{miss} = \mathcal{D}_{CCC}^{miss} \setminus \mathcal{D}_{valid}^{miss}$; /* Split */
- 8 **return** $\mathcal{D}_{train}^{miss}, \mathcal{D}_{valid}^{miss}$;

3.2 InformedAutoML

Building on the evidence in Section 1 that statistically informed data splitting significantly benefits actuarial modeling, we aim to evaluate the efficacy of a holistic IDPP and provide a practical actuarial modeling framework. To this end, we integrate IDPP into the existing *InsurAutoML* framework proposed by Dong and Quan (2025). This integration seeks to enhance both predictive performance and computational efficiency, resulting in a refined framework we designate as *InformedAutoML*.

Given the input dataset \mathcal{D}^{input} which has missing values, the complete training/validation set $(\mathcal{D}_{train}^{comp}, \mathcal{D}_{valid}^{comp}) = \mathcal{IDPP}^{comp}(\mathcal{D}^{input})$ and the missing training/validation set $(\mathcal{D}_{train}^{miss}, \mathcal{D}_{valid}^{miss}) = \mathcal{IDPP}^{miss}(\mathcal{D}^{input})$ are generated from the complete and missing IDPP respectively. The preprocessed datasets are then fed to model-only InsurAutoML, which entirely bypasses the previously designed preprocessing stages, including encoding, imputation, balancing, scaling, and feature selection. The model-only InsurAutoML optimizes the model architecture $f \in \mathcal{M}$ and the model hyperparameters $\lambda^M \in \Lambda^M$, where \mathcal{M} and Λ^M denote the space of model architecture and model hyperparameters, respectively. The complete and missing model-only optimization thus can be expressed as

$$\begin{aligned} f_{comp}^*, \lambda_{comp}^{M*} &= \operatorname{argmin}_{f \in \mathcal{M}, \lambda^M \in \Lambda^M} \mathbb{E}_{(\mathcal{D}_{train}^{comp}, \mathcal{D}_{valid}^{comp})} \mathcal{V}(\mathcal{L}, f_{\lambda^M}) \\ f_{miss}^*, \lambda_{miss}^{M*} &= \operatorname{argmin}_{f \in \mathcal{M}, \lambda^M \in \Lambda^M} \mathbb{E}_{(\mathcal{D}_{train}^{miss}, \mathcal{D}_{valid}^{miss})} \mathcal{V}(\mathcal{L}, f_{\lambda^M}) \end{aligned}$$

where \mathcal{L} denotes a certain loss function, \mathcal{V} denotes the evaluation process that trains an initiated model f_{λ^M} on the training set and returns the loss calculated on the validation set.

Given two sets of optimal model architecture and model hyperparameters, we adopt the following aggregation procedure to generate a final model prediction for any observation $\mathbf{x}_s \in \mathbb{R}^{1 \times p}$

$$\hat{y}_s = \begin{cases} f_{miss}^*(\mathcal{IDPP}^{miss}(\mathbf{x}_s); \lambda_{miss}^{M*}, \hat{\boldsymbol{\theta}}_{miss}), & \text{if } \mathbf{x}_s \text{ contains missing values} \\ \frac{1}{2}(f_{comp}^*(\mathcal{IDPP}^{comp}(\mathbf{x}_s); \lambda_{comp}^{M*}, \hat{\boldsymbol{\theta}}_{comp}) + f_{miss}^*(\mathcal{IDPP}^{miss}(\mathbf{x}_s); \lambda_{miss}^{M*}, \hat{\boldsymbol{\theta}}_{miss})), & \text{o.w.} \end{cases}$$

where $\hat{\boldsymbol{\theta}}_{comp}$ and $\hat{\boldsymbol{\theta}}_{miss}$ are the model parameters trained under the optimal settings for the complete and missing set, respectively. The workflow of the proposed InformedAutoML is illustrated in Figure 3. The proposed InformedAutoML framework is integrated into the InsurAutoML codebase.⁷

Although the complete and missing pipelines can be treated as off-the-shelf procedures applicable to arbitrary input datasets, both involve several hyperparameters, such as the missing threshold λ_{miss}^{comp} , the CCC feature selection threshold λ_{CCC}^{miss} , and the hyperparameters of the MissForest imputation, that influence preparation quality. We therefore incorporate optimization of these hyperparameters into the InsurAutoML framework as well. Intuitively, jointly

⁷<https://github.com/PanyiDong/InsurAutoML>

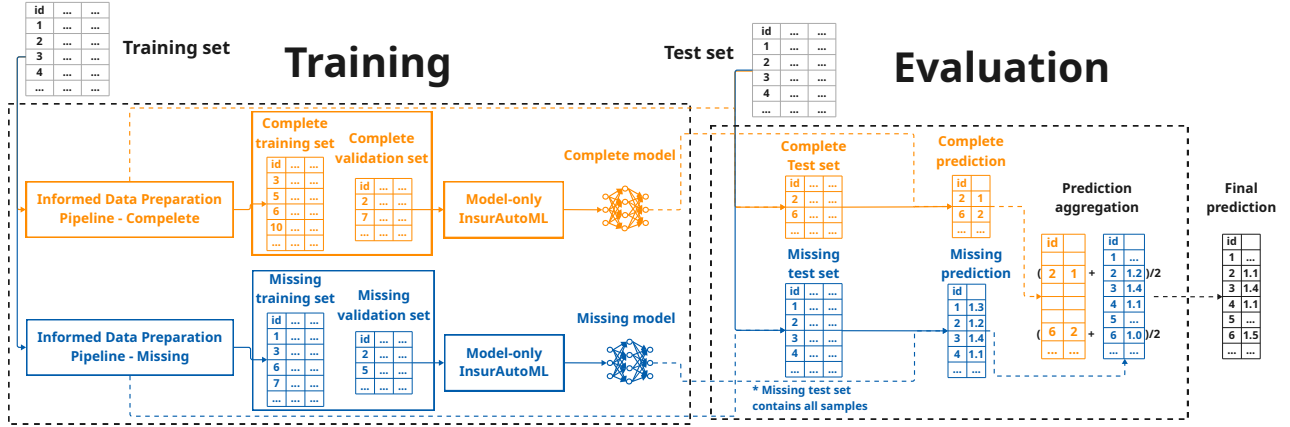


Figure 3: An illustration of InformedAutoML workflow

tuning the IDPP for each trial allows the fully tuned InformedAutoML to achieve superior performance at the expense of increased computational cost. In contrast, the model-tuning-only InformedAutoML is more computationally efficient, as the IDPP are applied only once; however, the fixed configuration may lead to suboptimal performance.

4 Experiments

To evaluate the efficacy of the proposed IDPP and InformedAutoML frameworks, we first conduct a controlled simulation study in Subsection 4.1, where the data generation process and underlying coefficients are known, allowing us to directly assess and benchmark the performance of IDPP. We then perform empirical experiments using InformedAutoML in Subsection 4.2 on two real-world datasets for which the true model specifications are unknown. In this case, the effectiveness of the proposed framework can only be evaluated through the performance of downstream predictive models.

4.1 Simulation Study

In this controlled simulation study, we introduce missing values under different missingness mechanisms into Tweedie-distributed datasets and apply the proposed IDPP. Using the resulting prepared datasets, we then attempt to recover the underlying Tweedie coefficients and compare with the simulation setting, allowing us to evaluate the effectiveness of the proposed framework.

4.1.1 Experiment Setup

Following the data generation process formulated in Appendix C.2, we first construct a simulated Tweedie-distributed dataset $\mathcal{D} = (\mathbf{X}, \mathbf{y})$. By introducing different mechanisms

of missingness, the fully observed dataset is then transformed into missing datasets $\mathcal{D}_{\text{mech}}^\Delta = (\mathbf{X}_{\text{mech}}^\Delta, \mathbf{y})$ where *mech* denotes one of the four missingness mechanisms, MCAR, MAR, MNAR and COMBO. Specifically, MCAR, MAR, and MNAR follow the definition in Rubin (1976); Rubin and Little (1987) and discussion in Subsection 2.3. The COMBO mechanism is a composition of the three missing mechanisms to reflect real-world scenarios. The missing value injection procedure for the four missing mechanisms is formulated in Appendix D. After applying the data preparation pipelines on the missing datasets, \mathcal{IDPP}^{comp} produces a complete training set $\mathcal{D}_{\text{mech},train}^{comp}$, while \mathcal{IDPP}^{miss} produces an missing training set $\mathcal{D}_{\text{mech},train}^{miss}$. It should be noted that the missing training set $\mathcal{D}_{\text{mech},train}^{miss}$ is imputed and therefore contains no missing values. Both pipelines apply CCC-based feature selection to choose the most informative features. Let $\hat{\mathcal{S}}_{\text{mech}}^{comp} \subseteq \{1, \dots, p\}$ and $\hat{\mathcal{S}}_{\text{mech}}^{miss} \subseteq \{1, \dots, p\}$ denote the indices of the features selected by the corresponding pipelines.

To evaluate parameter recovery performance for the complete pipelines \mathcal{IDPP}^{comp} , we fit a Tweedie GLM with the known Tweedie power q and dispersion φ parameters on $\mathcal{D}_{\text{mech},train}^{comp}$. Let $\hat{\beta}_{\text{mech}}^{comp}$ denote the estimated Tweedie coefficients and β^{true} represent the ground-truth coefficients. The accuracy of the estimated coefficients is then quantified via the Mean Absolute Error (MAE), defined as

$$\hat{\epsilon}_{\text{mech},MAE}^{comp} = \frac{1}{|\hat{\mathcal{S}}_{\text{mech}}^{comp}|} \sum_{j \in \mathcal{S}_{\text{mech}}^{comp}} |\hat{\beta}_{\text{mech},j}^{comp} - \beta_j^{\text{true}}|,$$

where $|\hat{\mathcal{S}}_{\text{mech}}^{comp}|$ is the cardinality of the selected feature set. We also report the number of real features retained, $|\hat{\mathcal{S}}_{\text{mech}}^{comp} \cap \mathcal{S}_{\text{Real}}|$, where $\mathcal{S}_{\text{Real}} = \{j : \beta_j^{\text{true}} \neq 0\}$ denotes the indices of informative features. Lower the MAE $\hat{\epsilon}_{\text{mech},MAE}^{comp}$ indicates more accurate coefficient estimation, while larger $|\hat{\mathcal{S}}_{\text{mech}}^{comp} \cap \mathcal{S}_{\text{Real}}|$ represents more comprehensive coverage of the selected features. For missing pipelines, corresponding MAE $\hat{\epsilon}_{\text{mech},MAE}^{miss}$ and feature coverage $|\hat{\mathcal{S}}_{\text{mech}}^{miss} \cap \mathcal{S}_{\text{Real}}|$ can be computed the same as complete pipelines by applying \mathcal{IDPP}^{miss} on the missing training set $\mathcal{D}_{\text{mech},train}^{miss}$. To ensure fair and comparable evaluation across the two pipelines, hyperparameters are tuned for both pipelines using grid search.

4.1.2 Result Analysis

Table 1 summarizes the experiment results across all 12 settings (3 datasets \times 4 missingness injection mechanisms). Please refer to Appendix E for the exact coefficients recovered under all settings. We can observe that $\hat{\epsilon}_{\text{mech},MAE}^{miss}$ is consistently lower than $\hat{\epsilon}_{\text{mech},MAE}^{comp}$ across all datasets and missingness mechanisms. This suggests that, by utilizing all available information, the imputation-based strategy can better capture the feature correlation and provide more accurate coefficient estimation. It should be noted that such an advantage can also be observed in the more challenging MNAR and COMBO cases, indicating that \mathcal{IDPP}^{miss} can more effectively mitigate the distribution distortion induced by missingness.

More specifically, the MAR and MNAR mechanisms in Data 3 exhibit more substantial improvements in coefficient estimation. Under the MAR mechanism, the MAE is reduced from

Dataset	Missingness	$IDPP^{comp}$			$IDPP^{miss}$		
		$\hat{\epsilon}_{mech,MAE}^{comp}$	$ \hat{\mathcal{S}}_{mech}^{comp} $	$ \hat{\mathcal{S}}_{mech}^{comp} \cap \mathcal{S}_{Real} $	$\hat{\epsilon}_{mech,MAE}^{miss}$	$ \hat{\mathcal{S}}_{mech}^{miss} $	$ \hat{\mathcal{S}}_{mech}^{miss} \cap \mathcal{S}_{Real} $
Data 1	MCAR	0.0081	4	3	0.0031	3	2
	MAR	0.0122	3	3	0.0057	1	1
	MNAR	0.0153	2	2	0.0114	4	3
	COMBO	0.0104	2	2	0.0010	1	1
Data 2	MCAR	0.0145	1	1	0.0084	1	1
	MAR	0.0306	2	2	0.0235	4	3
	MNAR	0.0255	4	3	0.0248	4	3
	COMBO	0.0199	4	3	0.0194	4	3
Data 3	MCAR	0.0553	3	2	0.0505	6	5
	MAR	0.0973	4	2	0.0356	6	4
	MNAR	0.0649	4	2	0.0359	3	3
	COMBO	0.0116	6	4	0.0106	6	4

Table 1: Summary of coefficient estimation on the training set

0.0973 to 0.0356, while under the MNAR mechanism, it decreases from 0.0649 to 0.0359 when the missing pipelines are utilized. This improvement is largely driven by the high level of missingness in the dataset. As reported in Table 6, Appendix D, the row-wise missingness rate is approximately 74.11%–75.71% across all mechanisms in Data 3. Because $IDPP^{comp}$ relies on complete-case filtering, it is forced to operate on a substantially smaller subset of observations, thereby weakening its ability to recover the underlying coefficients as other complete case analyses. In contrast, $IDPP^{miss}$ can leverage the imputed data to retain more informative features. For example, under the MAR mechanism in Data 3, $IDPP^{comp}$ retains only two informative features, whereas $IDPP^{miss}$ retains four. These results suggest that $IDPP^{miss}$ better preserves informative features and achieves more stable coefficient recovery in high missingness settings.

At the same time, $IDPP^{miss}$ often retains more informative features under missingness, as reflected by larger values of $|\hat{\mathcal{S}}_{mech}^{miss} \cap \mathcal{S}_{Real}|$. This pattern is particularly pronounced in the higher-missingness settings, Data 3, where $IDPP^{miss}$ retains substantially more informative features than $IDPP^{comp}$. However, retaining more informative features does not necessarily imply more accurate coefficient recovery. As shown in Data 1, $IDPP^{comp}$ sometimes retains as many as or more informative features than $IDPP^{miss}$, yet $IDPP^{miss}$ still achieves lower MAE. For example, under MCAR for Data 1, $IDPP^{comp}$ retains more informative features than $IDPP^{miss}$, with $|\hat{\mathcal{S}}_{mech}^{comp} \cap \mathcal{S}_{Real}| = 3$ compared with $|\hat{\mathcal{S}}_{mech}^{miss} \cap \mathcal{S}_{Real}| = 2$, yet $IDPP^{miss}$ still performs better in coefficient estimation, achieving MAE of 0.0031 compared to 0.0081 in the complete pipeline. A possible reason is that $IDPP^{comp}$ relies only on the fully observed subset, the resulting training dataset may be less representative of the underlying distribution, leading to less accurate recovery of the true coefficients.

Overall, these results indicate that the imputation-based strategy can better preserve informative features under high missingness rates and more stably recover the corresponding coefficients, even in cases where the number of retained informative features is lower than that

of the complete pipeline.

4.2 Real-world Study

We then compare InformedAutoML performance against the original InsurAutoML framework. Because model architectures, ensemble strategies, and hyperparameter tuning procedures are held identical to those in InsurAutoML, any observed performance improvements in InformedAutoML can be attributed solely to the proposed IDPP. Specifically, we conduct two experiments: one on a complete dataset, the Australian automobile insurance dataset (*ausprivauto*) (De Jong et al., 2008), and another on a dataset with missing values, the U.S. college Pell Grant dataset⁸ obtained from OpenML (Bischl et al., 2025).

4.2.1 Complete Data

For the complete datasets, since no missing values are present and no imputation is required, only the complete IDPP and complete model optimization components (the orange modules in Figures 2 and 3) are activated, and prediction aggregation is not performed. The *ausprivauto* dataset is one of the three insurance datasets have been analyzed in Dong and Quan (2025) and contains 67,856 automobile insurance policies. We use claim amount as the response variable, formulating a regression task. The exact same train–test split and the same Mean Squared Error (MSE) evaluation metric, which writes

$$\hat{\epsilon}_{MSE}^{train} = \frac{1}{N_{train}} \sum_{i=1}^{N_{train}} (y_i^{train} - f(\mathbf{X}_i^{train}; \hat{\theta}))^2, \quad \hat{\epsilon}_{MSE}^{test} = \frac{1}{N_{test}} \sum_{j=1}^{N_{test}} (y_j^{test} - f(\mathbf{X}_j^{test}; \hat{\theta}))^2$$

are adopted as in Dong and Quan (2025), enabling a direct comparison between InformedAutoML and prior results. We further evaluate the proposed framework under varying budget settings, where G denotes the evaluation budget in terms of the number of trials and T represents the time budget specifying the maximum allowable runtime. Larger values of G and T enable more thorough optimization and generally lead to improved performance metrics, with increased computational cost. The results are summarized in Table 2 and Figure 4.

As shown in Table 2, InformedAutoML generally follows the same trend as InsurAutoML, with both training and test performance improving as the evaluation budget increases, accompanied by longer runtimes for larger budgets. Notably, because only model optimization is activated, InformedAutoML is substantially more computationally efficient, typically achieving runtimes that are four to five times faster than those of InsurAutoML. Moreover, InformedAutoML generally outperforms InsurAutoML on both training and test metrics (highlighted in bold), with two exceptions: the training performance at $G = 8$ and the test performance at $G = 1024$. The former can be attributed to early-stage model misspecification, as evidenced by a pronounced training–test performance gap, while the latter arises because the reduced hyperparameter search space, resulting from model-only optimization, increases the likelihood of

⁸<https://www.openml.org/search?type=data&status=active&id=42727>

G	T/s	Model	runtime/s	Train MSE	Test MSE
8	900	InsurAutoML	952.30	993,285.74	1,220,835.99
		InformedAutoML	294.69	1,098,973.61	1,191,695.06
16	1,800	InsurAutoML	1,290.22	1,101,871.13	1,192,769.13
		InformedAutoML	606.11	1,092,658.21	1,191,822.05
32	3,600	InsurAutoML	2,181.53	1,099,855.88	1,191,872.59
		InformedAutoML	672.83	1,098,643.36	1,191,755.57
64	7,200	InsurAutoML	2,350.45	1,099,573.20	1,191,859.57
		InformedAutoML	1,468.66	1,091,833.70	1,191,615.84
128	14,400	InsurAutoML	4,274.43	1,099,296.76	1,191,913.62
		InformedAutoML	1,662.42	1,095,738.55	1,191,448.50
256	28,800	InsurAutoML	8,797.69	1,098,746.18	1,191,618.57
		InformedAutoML	2,042.39	1,095,817.06	1,191,298.75
512	57,600	InsurAutoML	11,533.74	1,098,873.21	1,192,162.05
		InformedAutoML	2,748.20	1,091,305.11	1,190,586.72
1024	115,200	InsurAutoML	23,347.84	1,098,817.89	1,191,450.96
		InformedAutoML	2,976.66	1,085,819.19	1,192,445.55

Red for best among all budget settings, **bold** for InsurAutoML vs InformedAutoML

Table 2: Performance on ausprivauto claim amount

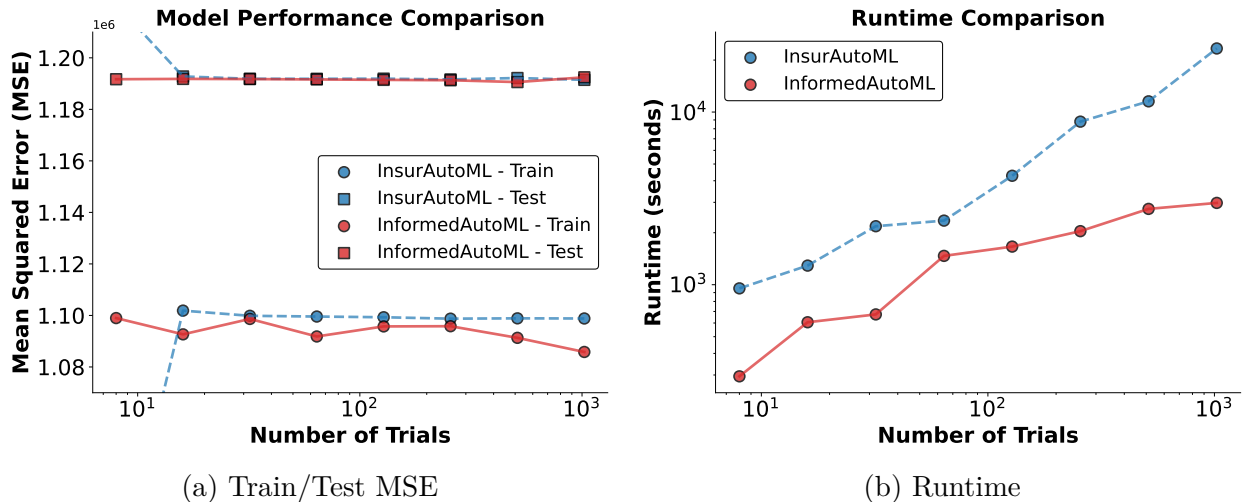


Figure 4: Train/Test MSE and runtime on ausprivauto claims dataset

overfitting, reflected in superior training performance at $G = 1024$. Importantly, InformedAutoML attains the globally optimal test performance at $G = 512$ (highlighted in red) earlier than $G = 1024$. This complete data analysis demonstrates that the proposed IDPP effectively prepare the data for improved predictive performance while enabling more efficient model deployment.

4.2.2 Missing Data

As the preceding experiments evaluate only subsets of the proposed IDPP, we next assess the full pipelines using a dataset with missing values: the U.S. college Pell Grant dataset. This dataset contains 7,063 observations and 45 features (including the response variable), where the response variable, *percent_pell_grant*, represents the proportion of undergraduates receiving Pell Grants at each institution. The covariates include institution information such as university location, SAT scores of enrolled students, graduate earnings, and Carnegie Classification. A 90–10 train–test split is applied, yielding a training set of 6,356 observations and a test set of 707 observations. We then follow the same experimental procedure by evaluating both InsurAutoML and InformedAutoML under varying budget settings, with the additional restriction that model architectures are limited to successful models selected by AutoGluon (Erickson et al., 2020) for this dataset, such as LightGBM (Ke et al., 2017), XGBoost (Chen and Guestrin, 2016), and ExtraTrees from scikit-learn (Pedregosa et al., 2011) for efficiency and performance considerations. In addition to evaluating performance on the original full training/test sets (denoted as *Missing* in Table 3), we also report results for the subset of observations retained in the complete set (denoted as *Complete* in Table 3). Although observations in the complete set may still contain some missing values, due to feature removal during complete-case selection, the overall missingness is low, and the impact of imputation choice is minimal. This setting allows for a more comprehensive assessment of the complete and missing IDPP and validates the effectiveness of the aggregation procedure outlined in Equation 3.2. The performance is evaluated using Root Mean Squared Error (RMSE), which can be expressed as

$$\hat{\epsilon}_{RMSE}^{train} = \sqrt{\hat{\epsilon}_{MSE}^{train}}, \quad \hat{\epsilon}_{RMSE}^{test} = \sqrt{\hat{\epsilon}_{MSE}^{test}}.$$

The results are summarized in Table 3 and Figure 5.

As shown in Table 3, InformedAutoML remains highly computationally efficient and generally achieves superior performance compared to InsurAutoML, with the exception of the test metric at $G = 1024$, which can be attributed to the overfitting issue discussed earlier. This observation suggests that early stopping with respect to the computational budget is particularly important for InformedAutoML, as its more restricted hyperparameter search space increases the risk of overfitting at large budgets. Overall, InformedAutoML outperforms InsurAutoML on both the complete and missing subsets and attains globally optimal performance on both training and test sets. These results indicate that the proposed IDPP produces informative datasets that enable downstream models to better capture the underlying data structure. Moreover, while training performance improves gradually with budget for both frameworks, InformedAutoML achieves strong test performance with only a small number of trials, highlighting the importance of statistically informed feature selection and train–test splitting for generalization and further supporting the effectiveness of the proposed IDPP.

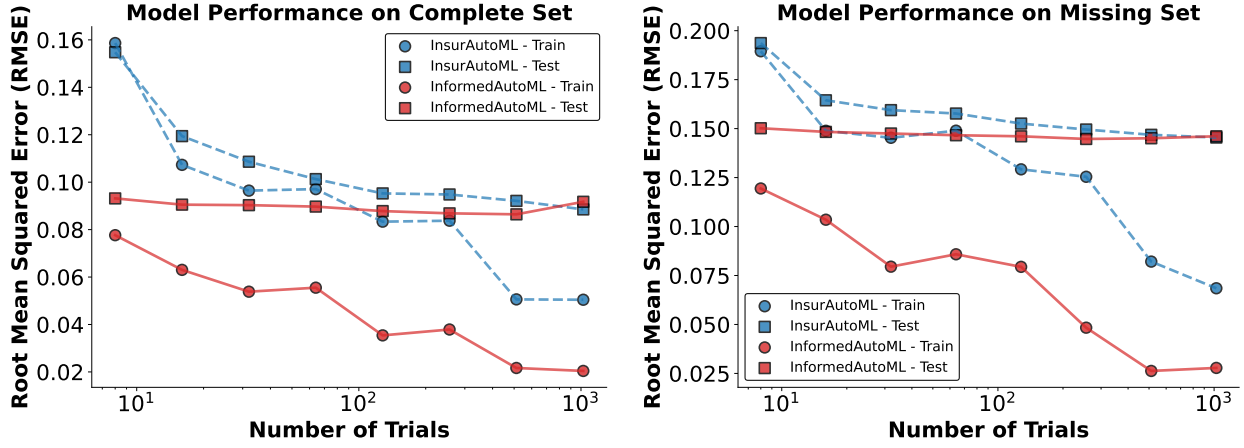
G	T/s	Model	runtime/s	Subset	Train RMSE	Test RMSE
8	900	InsurAutoML	1,072.68	Complete	0.1585	0.1545
				Missing	0.1895	0.1937
		InformedAutoML	69.10	Complete	0.0776	0.0932
				Missing	0.1194	0.1501
16	1,800	InsurAutoML	1,626.81	Complete	0.1073	0.1194
				Missing	0.1489	0.1594
		InformedAutoML	92.52	Complete	0.0630	0.0905
				Missing	0.1035	0.1483
32	3,600	InsurAutoML	2,817.34	Complete	0.0964	0.1086
				Missing	0.1453	0.1594
		InformedAutoML	153.60	Complete	0.0538	0.0903
				Missing	0.0795	0.1475
64	7,200	InsurAutoML	5,526.80	Complete	0.0971	0.1013
				Missing	0.1489	0.1577
		InformedAutoML	197.69	Complete	0.0555	0.0897
				Missing	0.0858	0.1466
128	14,400	InsurAutoML	8,724.71	Complete	0.0834	0.0953
				Missing	0.1292	0.1526
		InformedAutoML	414.60	Complete	0.0354	0.0878
				Missing	0.0794	0.1460
256	28,800	InsurAutoML	11,645.09	Complete	0.0838	0.0948
				Missing	0.1254	0.1495
		InformedAutoML	1,313.66	Complete	0.0379	0.0869
				Missing	0.0483	0.1447
512	57,600	InsurAutoML	27,466.38	Complete	0.0506	0.0921
				Missing	0.0821	0.1468
		InformedAutoML	2,841.35	Complete	0.0217	0.0864
				Missing	0.0263	0.1451
1024	115,200	InsurAutoML	41,499.85	Complete	0.0504	0.0885
				Missing	0.0685	0.1454
		InformedAutoML	3,576.04	Complete	0.0204	0.0917
				Missing	0.0278	0.1461

Red for best among all budget settings, **bold** for InsurAutoML vs InformedAutoML.

Table 3: Performance on college Pell Grant rate

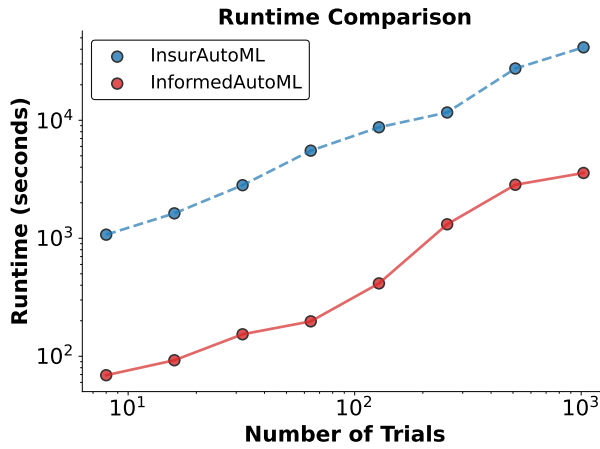
5 Conclusion

In this work, we examine the role and challenges of data preparation for highly imbalanced insurance data. In many actuarial applications, standard data preparation procedures, such as random train–test splitting, may lead to unstable model estimation and unreliable performance



(a) Train/Test RMSE on complete set

(b) Train/Test RMSE on missing set



(c) Runtime

Figure 5: Train/Test RMSE and runtime on college Pell Grant dataset

evaluation. To address this issue, we propose an informed data preparation framework that incorporates statistical methods for train–test splitting, feature selection, and missing data imputation. In particular, support points are employed to construct train–test splits that better preserve the distributional characteristics of the entire dataset. The Chatterjee correlation coefficient is used to identify informative features, while MissForest is adopted as a stable and reliable imputation method. This informed data preparation framework is further integrated into the InsurAutoML pipeline to form the InformedAutoML framework, which aims to provide efficient and effective predictive modeling for insurance data.

Empirical results from the controlled simulation study indicate that the proposed data preparation framework can extract representative information from datasets, leading to more stable and reliable downstream predictive models. Meanwhile, analysis on the behavior of these statistically informed data preparation methods suggests that they may require careful modification to align with the unique characteristics of insurance data. Experiments on both

complete and missing datasets using InformedAutoML further demonstrate that statistically informed data preparation can improve the efficiency, stability, and reliability of model training. These findings highlight that careful attention to data preparation can substantially improve predictive performance and computational efficiency, both of which are critical considerations in practical actuarial applications.

Despite these promising results, several limitations remain. First, the computational requirements of statistically informed data preparation tools often scale with dataset size, which may limit their applicability to very large insurance datasets. Second, while the data preparation process in InformedAutoML becomes more interpretable due to the statistical foundations of its components, the subsequent model optimization stage remains largely data-driven. Incorporating additional statistically informed mechanisms into the model optimization stage may further improve efficiency and transparency. Finally, although the proposed data preparation pipelines are designed for highly imbalanced settings, the downstream modeling procedures do not explicitly account for the imbalance in the prepared data. Developing model optimization strategies that consider imbalanced data distributions may further enhance the predictive performance of the InformedAutoML framework.

References

- Azadkia, M. and Chatterjee, S. (2021). A Simple Measure of Conditional Dependence. *The Annals of Statistics*, 49(6):3070–3102.
- Bischl, B., Casalicchio, G., Das, T., Feurer, M., Fischer, S., Gijbbers, P., Mukherjee, S., Müller, A. C., Németh, L., Oala, L., Purucker, L., Ravi, S., van Rijn, J. N., Singh, P., Vanschoren, J., van der Velde, J., and Wever, M. (2025). Openml: Insights from 10 years and more than a thousand papers. *Patterns*, 6(7):101317.
- Chatterjee, S. (2021). A new coefficient of correlation. *Journal of the American Statistical Association*, 116(536):2009–2022.
- Chen, T. and Guestrin, C. (2016). XGBoost: A scalable tree boosting system. In *Proceedings of the 22nd ACM SIGKDD International Conference on Knowledge Discovery and Data Mining*, pages 785–794. ACM.
- De Jong, P., Heller, G. Z., et al. (2008). *Generalized linear models for insurance data*. Cambridge University Press.
- Dong, P. and Quan, Z. (2025). Automated machine learning in insurance. *Insurance: Mathematics and Economics*, 120:17–41.
- Efromovich, S. (2017). What actuaries should know about nonparametric regression with missing data. *Variance*, 10(1):145–165.
- Erickson, N., Mueller, J., Shirkov, A., Zhang, H., Larroy, P., Li, M., and Smola, A. (2020). Autogluon-tabular: Robust and accurate AutoML for structured data. *arXiv preprint arXiv:2003.06505*.
- Fung, T. C., Tzougas, G., and Wüthrich, M. V. (2023). Mixture Composite Regression Models with Multi-type Feature Selection. *North American Actuarial Journal*, 27(2):396–428.
- Gan, G. and Yan, Y. (2025). Using neural networks for imputing missing values in insurance data. *Japanese Journal of Statistics and Data Science*, pages 1–39.
- Gomer, B. and Yuan, K.-H. (2021). Subtypes of the missing not at random missing data mechanism. *Psychological Methods*, 26(5):559.
- Höfling, H. and Tibshirani, R. (2008). A study of pre-validation. *The Annals of Applied Statistics*, 2(2):643 – 664.
- Jeong, H. (2022). Dimension reduction techniques for summarized telematics data. *The Journal of Risk Management*, 33:1–24.
- Ke, G., Meng, Q., Finley, T., Wang, T., Chen, W., Ma, W., Ye, Q., and Liu, T.-Y. (2017). LightGBM: A highly efficient gradient boosting decision tree. In *Advances in Neural Information Processing Systems*, volume 30.

- Little, R. J. (1993). Pattern-mixture models for multivariate incomplete data. *Journal of the American Statistical Association*, 88(421):125–134.
- Liu, Z., Saha, D., and Liang, F. (2026). Bayesian smoothing and variable selection using variational automatic relevance determination. *Journal of Computational and Graphical Statistics*, (just-accepted):1–15.
- Loh, P.-L. and Wainwright, M. J. (2011). High-dimensional regression with noisy and missing data: Provable guarantees with non-convexity. *Advances in neural information processing systems*, 24.
- Loh, W.-Y., Eltinge, J., Cho, M. J., and Li, Y. (2019). Classification and regression trees and forests for incomplete data from sample surveys. *Statistica Sinica*, 29(1):431–453.
- Lord, F. M. (1955). Estimation of parameters from incomplete data. *Journal of the American Statistical Association*, 50(271):870–876.
- Lüdtke, O., Robitzsch, A., and West, S. G. (2020). Analysis of interactions and nonlinear effects with missing data: A factored regression modeling approach using maximum likelihood estimation. *Multivariate Behavioral Research*, 55(3):361–381.
- Mak, S. and Joseph, V. R. (2018). Support points. *The Annals of Statistics*, 46(6A):2562–2592.
- Mirzaei, A., Carter, S. R., Patanwala, A. E., and Schneider, C. R. (2022). Missing data in surveys: Key concepts, approaches, and applications. *Research in Social and Administrative Pharmacy*, 18(2):2308–2316.
- Mohan, K. and Pearl, J. (2021). Graphical models for processing missing data. *Journal of the American Statistical Association*, 116(534):1023–1037.
- Niederreiter, H. (1992). *Random number generation and quasi-Monte Carlo methods*. SIAM.
- Pedregosa, F., Michel, V., Grisel, O., Blondel, M., Prettenhofer, P., Weiss, R., Vanderplas, J., Cournapeau, D., Pedregosa, F., Varoquaux, G., Gramfort, A., Thirion, B., Grisel, O., Dubourg, V., Passos, A., Brucher, M., Perrot, M., and Édouard Duchesnay (2011). Scikit-learn: Machine learning in Python. *Journal of Machine Learning Research*, 12(85):2825–2830.
- Rosenberg, M. A., Yun, S., and Kim, K. (2024). Assessing Oral Health in U.S. Children and Its Impact on Disparities of Overall Health and Health Expenditures: An Application Using Two-Stage Clustering. *North American Actuarial Journal*, 28(4):909–924.
- Rubin, D. B. (1976). Inference and missing data. *Biometrika*, 63(3):581–592.
- Rubin, D. B. (2018). Multiple imputation. In *Flexible imputation of missing data, second edition*, pages 29–62. Chapman and Hall/CRC.
- Rubin, D. B. and Little, R. J. (1987). *Statistical analysis with missing data*, volume 2. Wiley New York.

- Shi, H., Drton, M., and Han, F. (2021). On the power of chatterjee’s rank correlation. *Biometrika*, 109(2):317–333.
- Shi, K. and Shi, P. (2024). A Sparse Deep Two-part Model for Nonlife Insurance Claims. *Variance*, 17(1).
- Siddique, J., Harel, O., and Crespi, C. M. (2012). Addressing missing data mechanism uncertainty using multiple-model multiple imputation: Application to a longitudinal clinical trial. *The Annals of Applied Statistics*, 6(4):1814 – 1837.
- Stekhoven, D. J. and Bühlmann, P. (2012). Missforest—non-parametric missing value imputation for mixed-type data. *Bioinformatics*, 28(1):112–118.
- Vakayil, A., Joseph, R., and Mak, S. (2022). *SPLit: Split a Dataset for Training and Testing*. R package version 1.2.
- Vakayil, A. and Joseph, V. R. (2022). Data twinning. *Statistical Analysis and Data Mining: The ASA Data Science Journal*, 15(5):598–610.
- Van Buuren, S. and Groothuis-Oudshoorn, K. (2011). mice: Multivariate imputation by chained equations in r. *Journal of Statistical Software*, 45(3):1–67.
- Wang, E. T., Chiang, S., Haneef, Z., Rao, V. R., Moss, R., and Vannucci, M. (2023). Bayesian non-homogeneous hidden Markov model with variable selection for investigating drivers of seizure risk cycling. *The Annals of Applied Statistics*, 17(1):333 – 356.

Appendix A Notations

Notation	Description
\mathcal{D}	a dataset
\mathbf{X}	fully observed feature matrix
\mathbf{X}_i	i th feature vector in \mathbb{R}^p
X_{ij}	the j -th covariate of \mathbf{X}_i (element of \mathbf{X})
X_{i1}	the single covariate of \mathbf{X}_i when $p = 1$
y_i	realized response value for the i th observation
\mathbf{y}	response vector $(y_1, \dots, y_N)^\top$
\mathcal{O}_i	the i th observation (\mathbf{X}_i, y_i) in \mathcal{D}
N	the number of the observation in \mathcal{D}
p	the number of the features in \mathcal{D}
\mathcal{F}	data distribution
f	a model
$\boldsymbol{\theta}$	model parameter for f
\mathcal{L}	a loss function
\mathcal{T}_j	j th observation in $\mathcal{D}^{\text{test}}$
ε	the generalization error for f
$\hat{\varepsilon}$	empirical (estimated) error for f
C	a constant
$\overline{\text{ED}}$	the energy distance
r_i, l_i	the rank statistics for y_i
$NN(i)$	the nearest neighbor index for \mathbf{X}_i
q	power parameter of the Tweedie distribution
K	Poisson-distributed frequency part in Tweedie representation
U_s	Gamma-distributed severity of the s th claim in Tweedie representation
κ	Poisson mean parameter in Tweedie representation
ξ	Gamma shape parameter in Tweedie representation
ζ	Gamma scale parameter in Tweedie representation
Y_{tweedie}	the response variable follow Tweedie distribution
μ	mean parameter of the Tweedie distribution
φ	dispersion parameter of the Tweedie distribution
U_{is}	Gamma-distributed severity of the s th claim in observation i
$IDPP$	informed data preparation pipeline
R_j	missing rate of j -th feature
λ	a hyperparameter of a algorithm
\mathbf{W}	feature selection matrix
\mathcal{M}	model architecture space
Λ^M	model hyperparameter space
\mathcal{V}	evaluation process
\mathbf{x}_s	feature vector of one observation

Continued on next page

Notation	Description
G	evaluation budget
T	time budget
β_{true}	true regression slope under the Tweedie mean model
AR(1)	autoregressive process of order one used to generate features
Δ	missingness mask matrix in $\{0, 1\}^{N \times p}$
δ_{ij}	missing indicator for the entry X_{ij}
\mathbf{X}^Δ	masked feature matrix after applying Δ
X_{ij}^Δ	the (i, j) -th entry of the masked matrix \mathbf{X}^Δ
$Q_q(\cdot)$	empirical q -quantile operator
$\mathcal{Z}_{\text{mech}}$	set of masking rules for each missing mechanism
\mathcal{Z}^{sub}	mechanism-specific rule subsets within the COMBO mechanism
Z	number of masking rules in the corresponding rule set, $Z = \mathcal{Z} $
z	rule index, $z = 1, \dots, Z$
a_z	target feature index in rule z
b_z	conditioning feature index in rule z
c_z	quantile level in rule z
π_z	masking probability in rule z
τ_z	rule-specific threshold
$\eta_i^{(\text{Poi})}$	frequency linear score for observation i
$\eta_i^{(\text{Gam})}$	severity linear score for observation i
$X_{i,\text{Real}}$	informative covariate subvector for observation i
\mathbf{w}_{Poi}	weight vector for the frequency feature
\mathbf{w}_{Gam}	weight vector for the severity feature
γ	signal multiplier
\mathcal{D}^Δ	masked input dataset $(\mathbf{X}^\Delta, \mathbf{y})$
$\mathcal{D}_{\text{train}}^{\text{comp}}$	training set produced by $\text{IDPP}^{\text{comp}}$
$\mathcal{D}_{\text{train}}^{\text{miss}}$	training set produced by $\text{IDPP}^{\text{miss}}$ (after imputation)
$\widehat{\mathcal{S}}^{\text{comp}}$	index set of retained features after $\text{IDPP}^{\text{comp}}$
$\widehat{\mathcal{S}}^{\text{miss}}$	index set of retained features after $\text{IDPP}^{\text{miss}}$
$\hat{\beta}_j^{\text{comp}}$	estimated coefficient for feature j from the Tweedie GLM fitted on $\mathcal{D}_{\text{train}}^{\text{comp}}$
$\hat{\beta}_j^{\text{miss}}$	estimated coefficient for feature j from the Tweedie GLM fitted on $\mathcal{D}_{\text{train}}^{\text{miss}}$
β_j^{true}	ground-truth coefficient for feature j in the data-generating process
$\mathcal{S}_{\text{Real}}$	index set of informative features, i.e., $\{j : \beta_j^{\text{true}} \neq 0\}$
$ \widehat{\mathcal{S}}^{\text{comp}} $	number of features retained by $\text{IDPP}^{\text{comp}}$
$ \widehat{\mathcal{S}}^{\text{miss}} $	number of features retained by $\text{IDPP}^{\text{miss}}$
$ \widehat{\mathcal{S}}^{\text{comp}} \cap \mathcal{S}_{\text{Real}} $	number of informative features retained by $\text{IDPP}^{\text{comp}}$
$ \widehat{\mathcal{S}}^{\text{miss}} \cap \mathcal{S}_{\text{Real}} $	number of informative features retained by $\text{IDPP}^{\text{miss}}$

Table 4: Notations

Appendix B Tweedie Distribution Construction

For power parameters $q \in (1, 2)$, the Tweedie distribution can be written as a compound Poisson–Gamma distribution. Let

$$K \sim \text{Poisson}(\kappa), \quad U_s \stackrel{\text{iid}}{\sim} \text{Gamma}(\xi, \zeta), \quad s = 1, \dots, K,$$

with K independent of $\{U_s\}$. The response variable

$$Y_{\text{tweedie}} = \sum_{s=1}^K U_s$$

has a point mass at zero when $K = 0$ and continuous positive support when $K > 0$. This representation captures both zero response variables and heavy-tailed positive values.

Under the mean–dispersion specification $\text{Tw}(\mu, \varphi, q)$, the Poisson–Gamma parameters are linked to the mean μ , dispersion φ , and power parameter q through

$$\kappa = \frac{\mu^{2-q}}{\varphi(2-q)}, \quad \xi = \frac{2-q}{q-1}, \quad \zeta = \varphi(q-1)\mu^{q-1}.$$

This parameterization yields

$$\mathbb{E}[Y_{\text{tweedie}}] = \mu, \quad \text{Var}(Y_{\text{tweedie}}) = \varphi \mu^q,$$

which characterizes the Tweedie family by its mean–variance relationship within a unified distributional framework.

Appendix C Simulation Design

A synthetic dataset is defined as $\mathcal{D} = \{\mathcal{O}_i = (\mathbf{X}_i, y_i)\}_{i=1}^N \in \mathbb{R}^{N \times (p+1)}$, where N is the number of observations, each consisting of a p -dimensional feature vector $\mathbf{X}_i = (X_{i1}, \dots, X_{ip}) \in \mathbb{R}^p$ and a response $y_i \in \mathbb{R}$. The full feature matrix is denoted by $\mathbf{X} \in \mathbb{R}^{N \times p}$ and the response vector by $\mathbf{y} = (y_1, \dots, y_N)^\top \in \mathbb{R}^N$.

We assume that observations are independently drawn from the Tweedie family,

$$(\mathbf{X}_i, y_i) \stackrel{\text{iid}}{\sim} \mathcal{F}_{\text{Tw}}, \quad i = 1, \dots, N,$$

where \mathcal{F}_{Tw} denotes the Tweedie distribution.

C.1 Univariate Tweedie Data

In this design $p = 1$, so that \mathbf{X}_i reduces to a single covariate X_{i1} generated from an autoregressive AR(1) process. Conditional on X_{i1} , the response variable is modeled as

$$Y_i | X_{i1} \sim \text{Tw}(m(X_{i1}), \varphi, q), \quad i = 1, \dots, N,$$

with Tweedie parameters fixed at $q = 1.95$ and $\varphi = 1.5$. Its realization is denoted by y_i , and the collection of realizations forms \mathbf{y} . Each random variable Y_i can be represented in compound Poisson–Gamma form as

$$Y_i = \sum_{s=1}^{K_i} U_{is}, \quad K_i \sim \text{Poisson}(\kappa), \quad U_{is} \stackrel{\text{iid}}{\sim} \text{Gamma}(\xi, \zeta),$$

with K_i independent of $\{U_{is}\}$. The parameters are calibrated through exponential link functions so that

$$\mathbb{E}[K_i] = 1 \quad \text{and} \quad \mathbb{E}[U_{is}] = 10,000.$$

This specification implies the conditional mean $\mathbb{E}[Y_i | X_{i1}] = m(X_{i1})$, and the calibration yields an implied regression slope of $\beta_{\text{true}} = 0.2252$.

We set $N = 10,000$, producing a dataset that reproduces both structural zeros (when $K_i = 0$) and extreme positive response variables (when $K_i > 0$), thereby reflecting the essential features of insurance claims data.

C.2 Multivariate Tweedie Data

For the controlled simulation study in Subsection 4.1, we extend the univariate Tweedie data introduced in Appendix C.1. Specifically, the dataset $\mathcal{D} = \{\mathcal{O}_i = (\mathbf{X}_i, y_i)\}_{i=1}^N$ has $N = 10,000$ observations and continuous feature vectors $\mathbf{X}_i \in \mathbb{R}^p$ ($p > 1$). To further mimic real-world scenarios, these features are then partitioned into *real* features (non-zero Tweedie coefficient)

that characterize both the frequency and severity components in the Tweedie distribution and *fake* features (coefficient of zero) that are irrelevant to the response and thus can be considered as noise. We utilize pre-specified weight vectors \mathbf{w}_{Poi} and \mathbf{w}_{Gam} for frequency and severity components respectively, and a signal multiplier $\gamma > 0$ to govern the overall signal strength. It should be noted that fake features have Poisson and Gamma coefficients of zero. Let $\eta_i^{(\text{Poi})}$ and $\eta_i^{(\text{Gam})}$ denote the corresponding linear scores, in the form

$$\eta_i^{(\text{Poi})} = \gamma \langle \mathbf{X}_i, \mathbf{w}_{\text{Poi}} \rangle, \quad \eta_i^{(\text{Gam})} = \gamma \langle \mathbf{X}_i, \mathbf{w}_{\text{Gam}} \rangle$$

The linear scores are then normalized following

$$\hat{\eta}_i^{(\text{Poi})} = \frac{N e^{0.2 + \eta_i^{(\text{Poi})}}}{\sum_{i=1}^N e^{0.2 + \eta_i^{(\text{Poi})}}}, \quad \hat{\eta}_i^{(\text{Gam})} = 10,000 \frac{N e^{6 + \eta_i^{(\text{Gam})}}}{\sum_{i=1}^N e^{6 + \eta_i^{(\text{Gam})}}}$$

so that $\mathbb{E}[K_i] = 1$ and $\mathbb{E}[U_{is}] = 10,000$ for the frequency and severity components, which is consistent with Appendix C.1. The calibration ensures that the expected frequency and severity reflect realistic claim behaviors. Under this structural design, the data has true Tweedie coefficient vector of $\beta_{\text{true}} = (2 - q)\mathbf{w}_{\text{Poi}} + (q - 1)\mathbf{w}_{\text{Gam}}$, with zero Tweedie coefficient for fake features.

To systematically evaluate model performance across varying feature dimensions, dispersion structures, and signal magnitudes, we configure three simulation datasets. In each configuration, the power parameter is held constant at $q = 1.85$, while the number of real/fake features, the dispersion parameter ϕ , and the signal multiplier γ are varied. The configuration details alongside the resulting empirical distributions of the response variable \mathbf{y} are summarized in Table 5.

Dataset	$(p_{\text{Real}}, p_{\text{Fake}})$	ϕ	Signal γ	β_{true} (real features)
Data 1	(3, 2)	1.5	1	(0.2865, 0.6165, 0.9465)
Data 2	(3, 2)	1.8	3	(0.8595, 1.8495, 2.8395)
Data 3	(6, 4)	1.8	1	(0.243, 0.573, 0.903, 1.233, 1.563, 1.893)

(a) Tweedie distribution parameters and the resulting true regression coefficients

Dataset	Non-zero Rate ($y > 0$)	95th Percentile ($Q_{0.95}$)	Count $> Q_{0.95}$
Data 1	96.29%	10,429.68	482
Data 2	53.19%	4,296.21	266
Data 3	67.10%	7,415.66	336

(b) Empirical distribution of the response variable

Table 5: Configurations and empirical summaries for the three simulated datasets

Appendix D Missingness Injection Mechanisms

Let $\mathbf{X} \in \mathbb{R}^{N \times p}$ denote the complete feature matrix generated based on Appendix C.2. We inject missing values to the feature matrix by generating a binary mask matrix $\Delta \in \{0, 1\}^{N \times p}$, where its element $\delta_{ij} = 1$ indicates that the j -th covariate of i -th observation X_{ij} is missing. Thus, the elements of the masked feature matrix \mathbf{X}^Δ follows

$$X_{ij}^\Delta = \begin{cases} \text{NA}, & \delta_{ij} = 1, \\ X_{ij}, & \delta_{ij} = 0, \end{cases} \quad i = 1, \dots, N, \quad j = 1, \dots, p.$$

We consider all three missingness mechanisms: MCAR, MAR, and MNAR, in our experiments. Additionally, we consider a mixed missingness setting, denoted as COMBO, to reflect real-world missing data characteristics. Each mechanism is characterized by a missingness rule set $\mathcal{Z}_{\text{mech}}$, (i.e., $\mathcal{Z}_{\text{MCAR}}$, \mathcal{Z}_{MAR} , $\mathcal{Z}_{\text{MNAR}}$ and $\mathcal{Z}_{\text{COMBO}}$) with $Z_{\text{mech}} = |\mathcal{Z}_{\text{mech}}|$ number of rules. For each mechanism, we first construct a rule-specific mask for every rule $z \in \mathcal{Z}_{\text{mech}}$, and then aggregate all rule-specific masks through their elementwise maximum.

Under MCAR, we set $Z_{\text{MCAR}} = p$ and define the missingness rule set as $\mathcal{Z}_{\text{MCAR}} = \{(a_z, \pi_z)\}_{z=1}^{Z_{\text{MCAR}}}$ where $a_z \in \{1, \dots, p\}$ denotes the target feature index to be partially masked and $\pi_z \in (0, 1)$ is the masking probability for the target feature. Thus, the elements of the mask matrix generated by z -th missingness rule $\Delta^{\text{MCAR},(z)}$ follows

$$\delta_{ij}^{\text{MCAR},(z)} \sim \text{Bernoulli}(\pi_z) \mathbb{1}_{\{j=a_z\}}, \quad i = 1, \dots, N, \quad j = 1, \dots, p.$$

The MCAR mask is then obtained by the elementwise maximum of all mask matrices:

$$\Delta^{\text{MCAR}} = \left(\delta_{ij}^{\text{MCAR}} \right)_{i=1, \dots, N; j=1, \dots, p} := \left(\max_{z \in \mathcal{Z}_{\text{MCAR}}} \delta_{ij}^{\text{MCAR},(z)} \right)_{i=1, \dots, N; j=1, \dots, p}.$$

In the MAR and MNAR schemes, masking rules depend on quantile thresholds of the conditioning features. The MAR missingness rule set is defined as $\mathcal{Z}_{\text{MAR}} = \{(a_z, b_z, c_z, \pi_z)\}_{z=1}^{Z_{\text{MAR}}}$ where $b_z \in \{1, \dots, p\}$ denotes the conditioning feature index that triggers the masking and $c_z \in (0, 1)$ is the quantile level. For z -th missingness rule, we first determine the empirical quantile of the conditioning feature b_z , $\tau_z^b = Q_{c_z}(\mathbf{X}_{\cdot, b_z})$, where Q_{c_z} denotes the c_z level of empirical quantile and \mathbf{X}_{\cdot, b_z} is the b_z -th feature. The elements of the corresponding rule-specific mask $\Delta^{\text{MAR},(z)}$ satisfies

$$\delta_{ij}^{\text{MAR},(z)} \sim \text{Bernoulli}(\pi_z) \mathbb{1}_{\{X_{i, b_z} < \tau_z^b\}} \mathbb{1}_{\{j=a_z\}}, \quad i = 1, \dots, N, \quad j = 1, \dots, p.$$

Thus, the missingness of feature a_z is conditional on the value of feature b_z . The MAR mask Δ^{MAR} can then be aggregated the same as the mask matrix of MCAR.

Under MNAR, the missingness of feature a_z depends on the value of the target feature itself. Thus, the missingness rule set is defined as $\mathcal{Z}_{\text{MNAR}} = \{(a_z, c_z, \pi_z)\}_{z=1}^{Z_{\text{MNAR}}}$. The corresponding

empirical quantile is defined as $\tau_z^a = Q_{c_z}(\mathbf{X}_{\cdot, a_z})$. The elements of the z -th rule-specific mask $\Delta^{\text{MNAR},(z)}$ follows

$$\delta_{ij}^{\text{MNAR},(z)} \sim \text{Bernoulli}(\pi_z) \mathbb{1}_{\{X_{i,a_z} < \tau_z^a\}} \mathbb{1}_{\{j=a_z\}}, \quad i = 1, \dots, N, \quad j = 1, \dots, p.$$

The MNAR mask Δ^{MNAR} takes the elementwise maximum of all missingness rules, the same as MCAR and MAR.

The missingness rule set of the COMBO mechanism is a mixed rule set following

$$\mathcal{Z}_{\text{COMBO}} = \cup_{\text{sub} \in \{\text{MCAR}, \text{MAR}, \text{MNAR}\}} \mathcal{Z}_{\text{COMBO}}^{\text{sub}}$$

where $\mathcal{Z}_{\text{COMBO}}^{\text{MCAR}} = \{(a_z^{\text{MCAR}}, \pi_z^{\text{MCAR}})\}_{z=1}^{\mathcal{Z}_{\text{COMBO}}^{\text{MCAR}}}$, $\mathcal{Z}_{\text{COMBO}}^{\text{MAR}} = \{(a_z^{\text{MAR}}, b_z^{\text{MAR}}, c_z^{\text{MAR}}, \pi_z^{\text{MAR}})\}_{z=1}^{\mathcal{Z}_{\text{COMBO}}^{\text{MAR}}}$ and $\mathcal{Z}_{\text{COMBO}}^{\text{MNAR}} = \{(a_z^{\text{MNAR}}, c_z^{\text{MNAR}}, \pi_z^{\text{MNAR}})\}_{z=1}^{\mathcal{Z}_{\text{COMBO}}^{\text{MNAR}}}$ denote the sub-missingness rule sets of the corresponding mechanisms in the COMBO mechanism. It should be noted that while the construction of $\mathcal{Z}_{\text{COMBO}}^{\text{sub}}$ is the same as the corresponding standalone rule sets, the exact rules are different. Following the construction of the mask matrices for MCAR, MAR, and MNAR mechanisms, we can construct three sub-mask matrices with elements $\delta_{ij}^{\text{sub}, \text{COMBO}}$ from corresponding sub-missing rule sets $\mathcal{Z}_{\text{COMBO}}^{\text{sub}}$. The elements of the COMBO mask matrix are then aggregated as

$$\delta_{ij}^{\text{COMBO}} = 1 - (1 - \delta_{ij}^{\text{MCAR}, \text{COMBO}})(1 - \delta_{ij}^{\text{MAR}, \text{COMBO}})(1 - \delta_{ij}^{\text{MNAR}, \text{COMBO}}), \quad i = 1, \dots, N, \quad j = 1, \dots, p.$$

Equivalently,

$$\Delta^{\text{COMBO}} = \left(\max\{\delta_{ij}^{\text{MCAR}, \text{COMBO}}, \delta_{ij}^{\text{MAR}, \text{COMBO}}, \delta_{ij}^{\text{MNAR}, \text{COMBO}}\} \right)_{i=1, \dots, N; j=1, \dots, p}.$$

The masked data matrix $\mathbf{X}_{\text{mech}}^\Delta$ for each missingness mechanism is constructed accordingly. The missingness rule sets are constructed such that the overall missing rates, $\frac{1}{pN} \sum_{i=1}^N \sum_{j=1}^p \delta_{ij}^{\text{mech}}$, remain close across all missing mechanisms. Tables 6–7 summarize row-wise and column-wise missingness rates for each of the three datasets under the three missing mechanisms (MCAR, MAR, MNAR) and the COMBO setting.

Dataset	MCAR	MAR	MNAR	COMBO
Data 1	11.30%	11.69%	11.83%	11.69%
Data 2	15.55%	15.62%	15.76%	15.79%
Data 3	74.50%	75.18%	74.11%	75.71%

Table 6: Row-wise missingness percentage

Dataset	Feature	MCAR	MAR	MNAR	COMBO
Data 1	RealCon1	3.19%	0.00%	0.00%	1.70%
	RealCon2	0.00%	0.00%	2.65%	1.47%
	RealCon3	4.69%	7.39%	2.59%	6.23%
	FakeCon1	0.00%	5.68%	6.03%	0.00%
	FakeCon2	3.79%	0.00%	3.54%	4.39%
	y	0.00%	0.00%	0.00%	0.00%
Data 1	RealCon1	3.19%	0.00%	0.00%	1.70%
	RealCon2	0.00%	0.00%	2.65%	1.47%
	RealCon3	4.69%	7.39%	2.59%	6.23%
	FakeCon1	0.00%	5.68%	6.03%	0.00%
	FakeCon2	3.79%	0.00%	3.54%	4.39%
	y	0.00%	0.00%	0.00%	0.00%
Data 2	RealCon1	4.69%	3.83%	0.00%	9.45%
	RealCon2	0.00%	3.42%	3.51%	3.36%
	RealCon3	6.28%	4.56%	5.02%	2.86%
	FakeCon1	0.00%	0.00%	6.59%	7.00%
	FakeCon2	5.48%	6.73%	3.54%	0.00%
	y	0.00%	0.00%	0.00%	0.00%
Data 3	RealCon1	9.45%	20.09%	20.01%	14.31%
	RealCon2	15.95%	11.99%	17.99%	29.85%
	RealCon3	18.14%	25.10%	29.73%	31.60%
	RealCon4	14.79%	18.15%	23.54%	0.00%
	RealCon5	19.03%	48.89%	49.27%	15.95%
	RealCon6	0.00%	0.00%	0.00%	0.00%
	FakeCon1	15.26%	18.03%	18.97%	15.22%
	FakeCon2	18.19%	16.29%	19.51%	32.80%
	FakeCon3	15.29%	15.67%	19.68%	14.79%
	FakeCon4	0.00%	0.00%	0.00%	0.00%
y	0.00%	0.00%	0.00%	0.00%	

The response variable y is kept fully observed across all experiments.

Table 7: Column-wise missingness rates percentage

Appendix E Coefficient-Level Recovery Results

Mechanism	Feature	True β	Fitted $\hat{\beta}$ on full data	$IDPP^{complete} \hat{\beta}$	$IDPP^{miss} \hat{\beta}$
Data 1					
MCAR	RealCon1	0.2865	0.2923	0.2891	–
	RealCon2	0.6165	0.6301	0.6321	0.6144
	RealCon3	0.9465	0.9327	0.9331	0.9506
	FakeCon1	0.0000	-0.0116	–	–
	FakeCon2	0.0000	-0.0132	0.0010	–
MAR	RealCon1	0.2865	0.2923	0.2911	–
	RealCon2	0.6165	0.6301	0.6481	–
	RealCon3	0.9465	0.9327	0.9462	0.9522
	FakeCon1	0.0000	-0.0116	–	–
	FakeCon2	0.0000	-0.0132	–	–
MNAR	RealCon1	0.2865	0.2923	–	0.2967
	RealCon2	0.6165	0.6301	0.6247	0.6336
	RealCon3	0.9465	0.9327	0.9242	0.9466
	FakeCon1	0.0000	-0.0116	–	–
	FakeCon2	0.0000	-0.0132	–	-0.0181
COMBO	RealCon1	0.2865	0.2923	–	–
	RealCon2	0.6165	0.6301	0.6293	–
	RealCon3	0.9465	0.9327	0.9385	0.9455
	FakeCon1	0.0000	-0.0116	–	–
	FakeCon2	0.0000	-0.0132	–	–
Data 2					
MCAR	RealCon1	0.8595	0.8079	–	–
	RealCon2	1.8495	1.8431	–	–
	RealCon3	2.8395	2.8386	2.8540	2.8479
	FakeCon1	0.0000	0.0194	–	–
	FakeCon2	0.0000	0.0052	–	–
MAR	RealCon1	0.8595	0.8079	–	0.8414
	RealCon2	1.8495	1.8431	1.8590	1.8861
	RealCon3	2.8395	2.8386	2.8913	2.8762
	FakeCon1	0.0000	0.0194	–	-0.0027
	FakeCon2	0.0000	0.0052	–	–
MNAR	RealCon1	0.8595	0.8079	0.8008	0.7974
	RealCon2	1.8495	1.8431	1.8498	1.8623
	RealCon3	2.8395	2.8386	2.8189	2.8559
	FakeCon1	0.0000	0.0194	0.0226	0.0078
	FakeCon2	0.0000	0.0052	–	–
COMBO	RealCon1	0.8595	0.8079	0.8073	0.8315
	RealCon2	1.8495	1.8431	1.8229	1.8855
	RealCon3	2.8395	2.8386	2.8395	2.8517
	FakeCon1	0.0000	0.0194	-0.0009	-0.0014

Continued on next page

Continued from previous page

Mechanism	Feature	True β	Fitted $\hat{\beta}$ on full data	$IDPP^{complete}$ $\hat{\beta}$	$IDPP^{miss}$ $\hat{\beta}$
	FakeCon2	0.0000	0.0052	–	–
Data 3					
MCAR	RealCon1	0.2430	0.2416	–	–
	RealCon2	0.5730	0.5784	–	0.6136
	RealCon3	0.9030	0.9032	–	1.0175
	RealCon4	1.2330	1.2225	1.2580	1.3116
	RealCon5	1.5630	1.5309	–	1.6123
	RealCon6	1.8930	1.8849	1.9661	1.8952
	FakeCon1	0.0000	0.0387	–	–
	FakeCon2	0.0000	-0.0104	–	–
	FakeCon3	0.0000	-0.0031	–	–
	FakeCon4	0.0000	-0.0011	0.0679	0.0177
MAR	RealCon1	0.2430	0.2416	–	0.2908
	RealCon2	0.5730	0.5784	0.5674	0.6602
	RealCon3	0.9030	0.9032	–	–
	RealCon4	1.2330	1.2225	–	1.2815
	RealCon5	1.5630	1.5309	–	–
	RealCon6	1.8930	1.8849	1.9488	1.9168
	FakeCon1	0.0000	0.0387	–	–
	FakeCon2	0.0000	-0.0104	–	–
	FakeCon3	0.0000	-0.0031	0.0717	-0.0030
	FakeCon4	0.0000	-0.0011	0.2560	0.0034
MNAR	RealCon1	0.2430	0.2416	–	–
	RealCon2	0.5730	0.5784	0.6660	0.6475
	RealCon3	0.9030	0.9032	–	–
	RealCon4	1.2330	1.2225	–	1.2638
	RealCon5	1.5630	1.5309	–	–
	RealCon6	1.8930	1.8849	1.8605	1.8905
	FakeCon1	0.0000	0.0387	0.0371	–
	FakeCon2	0.0000	-0.0104	–	–
	FakeCon3	0.0000	-0.0031	–	–
	FakeCon4	0.0000	-0.0011	0.0972	–
COMBO	RealCon1	0.2430	0.2416	0.2259	0.2563
	RealCon2	0.5730	0.5784	–	–
	RealCon3	0.9030	0.9032	–	–
	RealCon4	1.2330	1.2225	1.2378	1.2441
	RealCon5	1.5630	1.5309	1.5460	1.5658
	RealCon6	1.8930	1.8849	1.8773	1.8810
	FakeCon1	0.0000	0.0387	0.0004	0.0229
	FakeCon2	0.0000	-0.0104	–	–
	FakeCon3	0.0000	-0.0031	–	–
	FakeCon4	0.0000	-0.0011	-0.0143	0.0017

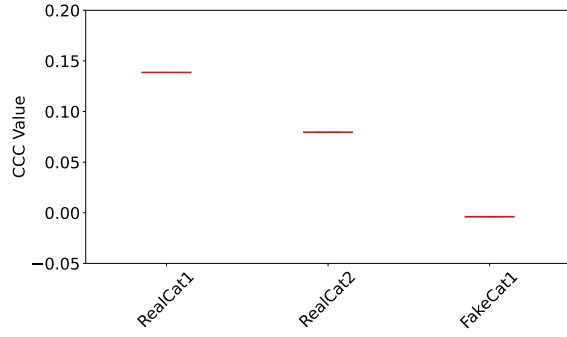
Table 8: Coefficient-level recovery results

Appendix F Discussion on Tie-breaking in CCC

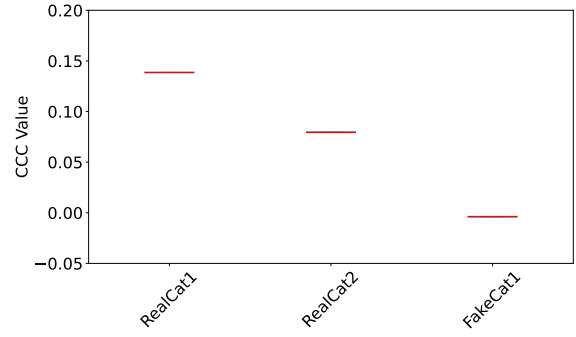
As discussed in Subsection 2.2, we employ CCC and ACCC to quantify feature dependence and identify informative variables for selection, noting that ties can introduce variability in the resulting correlation estimates. To illustrate this effect, we consider a simulated dataset generated according to the procedures described in Appendices B and C.2. The dataset includes three continuous variables (*RealCon1*, *RealCon2*, *FakeCon1*) and three categorical variables (*RealCat1*, *RealCat2*, *FakeCat1*). We examine three tie scenarios: (1) ties occurring only in \mathbf{X} , (2) ties occurring only in \mathbf{y} , and (3) ties occurring in both \mathbf{X} and \mathbf{y} . For each scenario, we evaluate four tie-breaking strategies: maximal, ordinal, random, and random-noise tie-breaking. Maximal tie-breaking assigns all tied values the maximum rank they would jointly occupy (e.g., three tied zeros that could receive ranks 1, 2, and 3 are all assigned rank 3). Ordinal tie-breaking assigns ranks according to the order of appearance in the dataset (e.g., if the tied observations appear at indices 4, 2, and 6, they are assigned ranks 2, 1, and 3, respectively). Random tie-breaking assigns ranks to tied values at random. Random-noise tie-breaking eliminates ties by adding zero-mean, extremely small-variance noise (here, Gaussian noise $\mathcal{N}(0, 1e^{-3})$) to the data, minimally perturbing the original values while removing ties at the source. It is worth noting that maximal and ordinal tie-breaking are deterministic for a fixed dataset, although shuffling the data can change ordinal assignments. In contrast, random and random-noise tie-breaking introduce stochasticity and can therefore induce variability in correlation estimates. To account for this, in addition to reporting single-run estimates, we repeat each estimation procedure 20 times and use the averaged correlation as the final estimate, which substantially reduces variability.

In the simulated dataset, ties arise only in the three categorical features, whereas the three continuous features take unique values. For the response variable, approximately 90% of observations are zeros (forming ties), while the remaining 10% are unique continuous values. Accordingly, we construct three experimental scenarios. For the case where ties exist only in \mathbf{X} , we select the three categorical features and restrict the analysis to observations with nonzero responses to avoid the ties (zeros) in \mathbf{y} . For the case where ties exist only in \mathbf{y} , we select all observations together with the three continuous features to avoid the ties in the three categorical features for \mathbf{X} . For the case where both \mathbf{X} and \mathbf{y} contain ties, we select the three categorical features and the full response variable. In the scenario where both \mathbf{X} and \mathbf{y} contain ties, we fix random tie-breaking for \mathbf{X} and examine the effect of different tie-breaking strategies applied to \mathbf{y} . For each scenario, we repeat the correlation estimation 50 times to assess variability. Under this setup, Figures 6, 7, and 8 summarize the results for the three tie scenarios. The results clearly show that deterministic tie-breaking strategies, such as maximal and ordinal tie-breaking, introduce no variability, as reflected by identical estimates across repetitions in Figure 6(a) and 7(a); consequently, averaging over multiple runs has no effect as illustrated in Figure 6(b) and 7(d). In contrast, when random or random-noise tie-breaking is employed, the estimated correlations exhibit noticeable variability (e.g., Figure 6(e) and 8(g)). This variability is substantially reduced when repeated estimations are averaged (e.g., Figure 6(f) and 8(h)). However, the proportion of ties also plays a critical role in estimating the impact of tie-breaking.

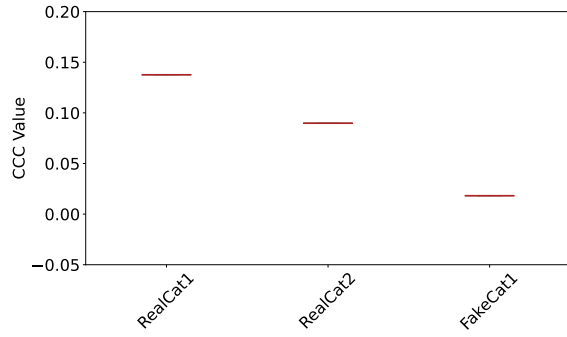
When ties are excessive, the induced variability can be substantial, rendering simple averaging less effective, as illustrated in Figure 7(f) and 7(h), where approximately 90% of the observations are tied. Such extreme proportion of ties also substantially affects the magnitude of the estimated correlations, driving the correlation values toward zero for all features, as illustrated in Figure 7. Moreover, random-noise tie-breaking behaves very similarly to random tie-breaking once averaging is applied, indicating that repetition and averaging are crucial for stabilizing correlation estimates under stochastic tie-breaking schemes. We observe similar behaviors in ACCC estimations. Based on these observations and additional experiments across different datasets, we adopt an average over 20 independent repetitions with random tie-breaking for \mathbf{X} and ordinal tie-breaking for \mathbf{y} as the final procedure for feature correlation estimation.



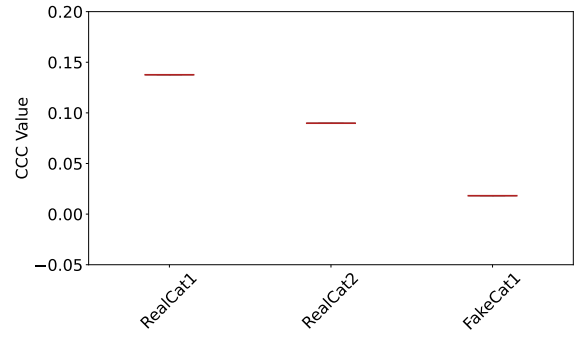
(a) Max tie breaking and 1 run



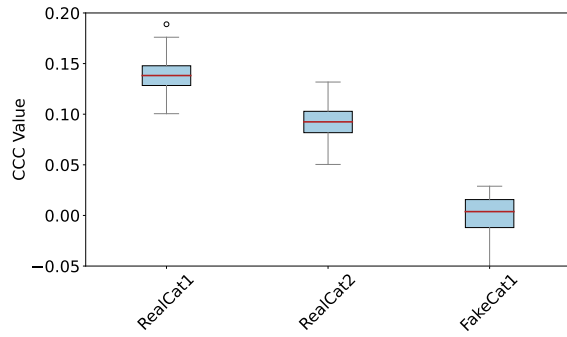
(b) Max tie breaking and 20 runs



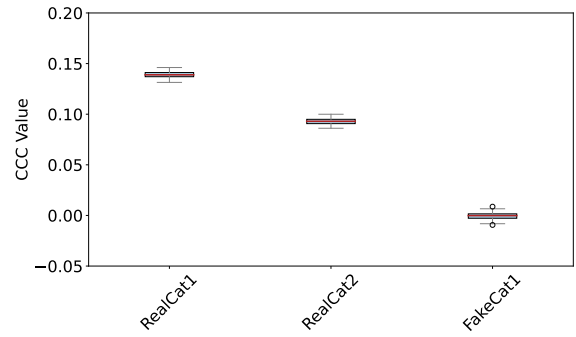
(c) Ordinal tie breaking and 1 run



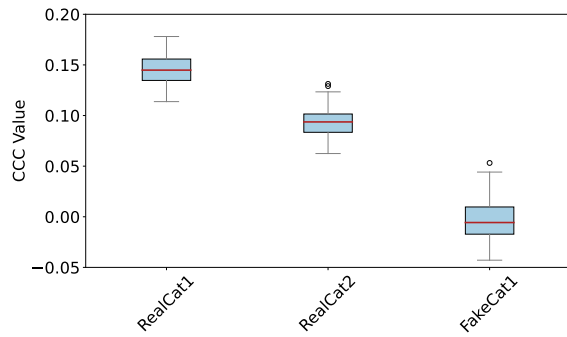
(d) Ordinal tie breaking and 20 runs



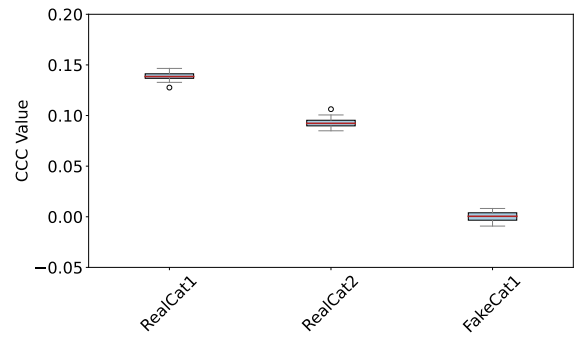
(e) Random tie breaking and 1 runs



(f) Random tie breaking and 20 runs

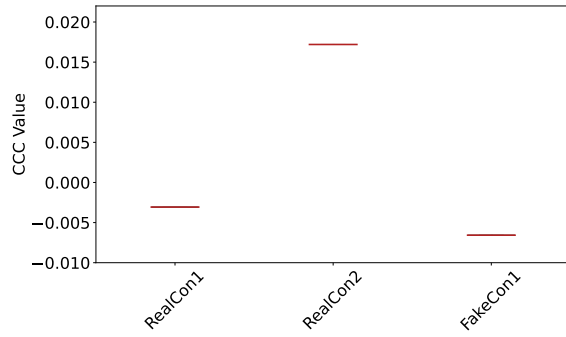


(g) Random noise tie breaking and 1 run

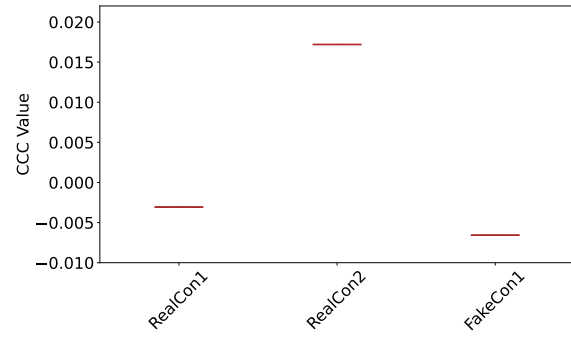


(h) Random noise tie breaking and 20 runs

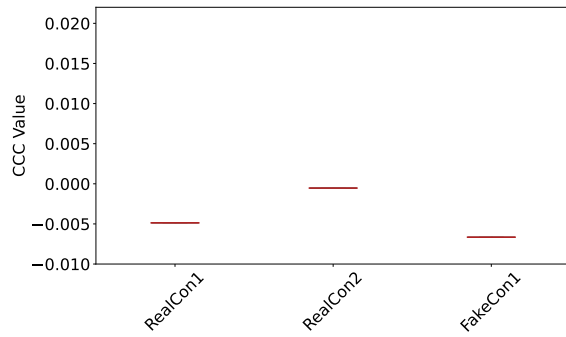
Figure 6: Comparison of CCC values on tie breaking when only \mathbf{X} has ties



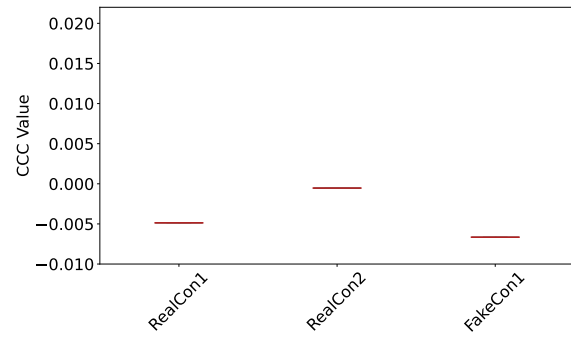
(a) Max tie breaking and 1 run



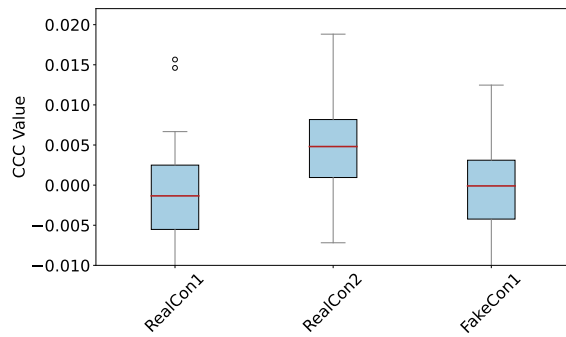
(b) Max tie breaking and 20 runs



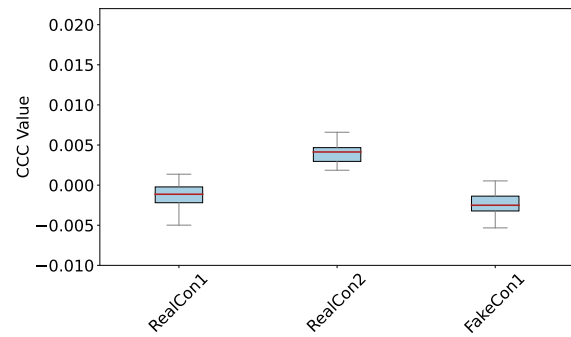
(c) Ordinal tie breaking and 1 run



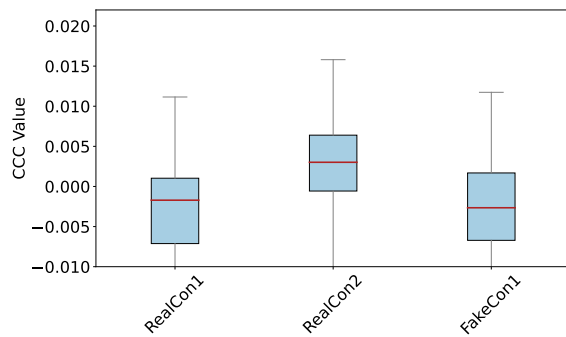
(d) Ordinal tie breaking and 20 runs



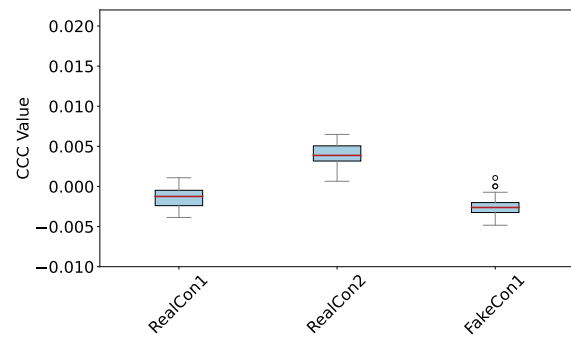
(e) Random tie breaking and 1 runs



(f) Random tie breaking and 20 runs

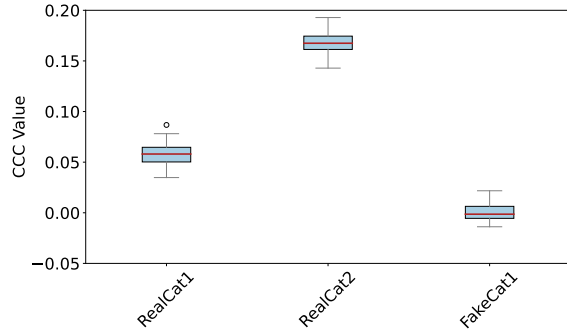


(g) Random noise tie breaking and 1 run

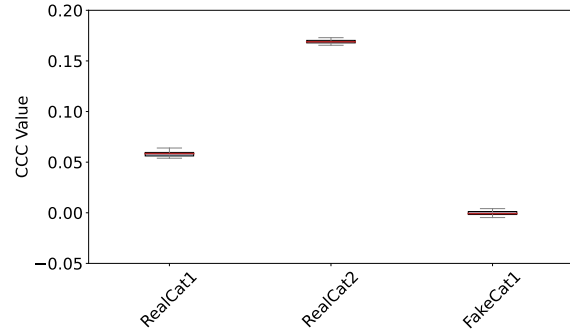


(h) Random noise tie breaking and 20 runs

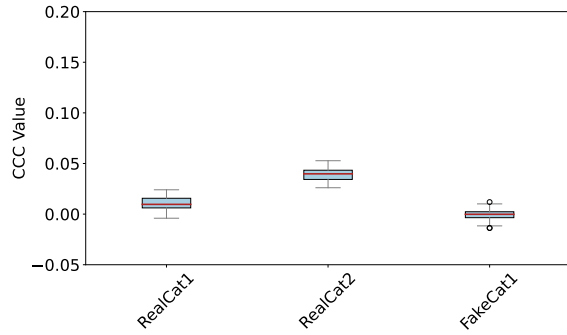
Figure 7: Comparison of CCC values on tie breaking when only \mathbf{y} has ties



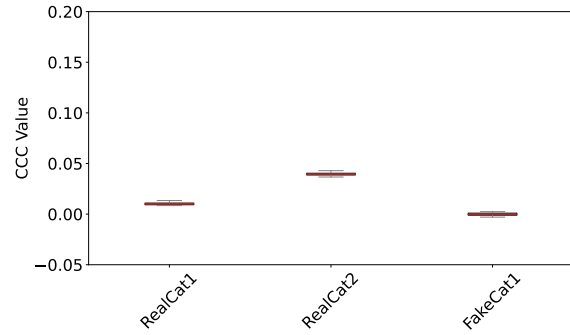
(a) Max tie breaking on \mathbf{y} and 1 run



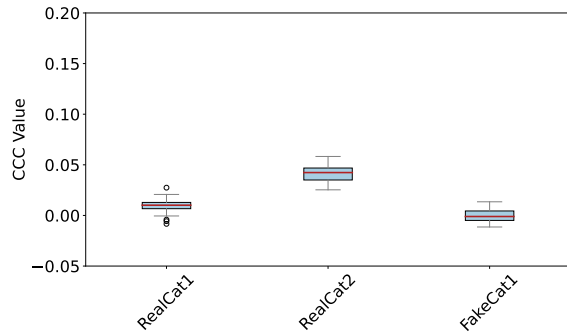
(b) Max tie breaking on \mathbf{y} and 20 runs



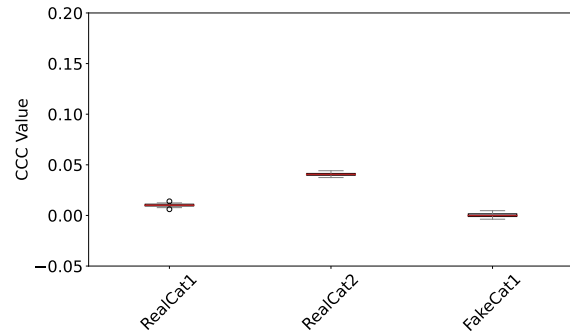
(c) Ordinal tie breaking on \mathbf{y} and 1 run



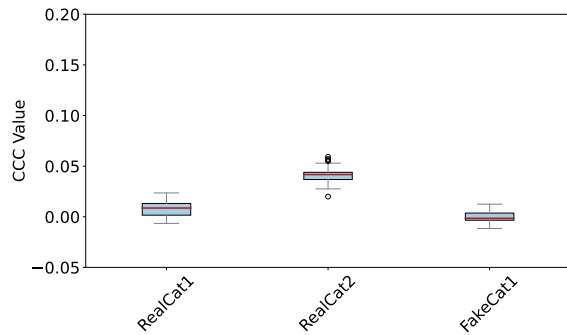
(d) Ordinal tie breaking on \mathbf{y} and 20 runs



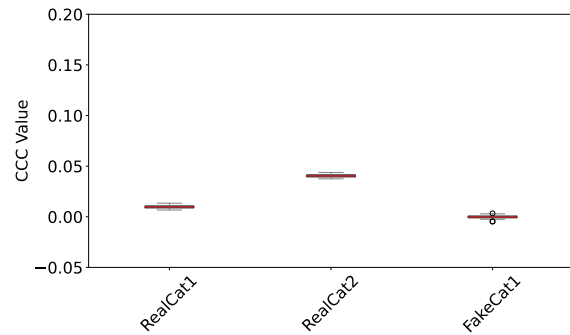
(e) Random tie breaking on \mathbf{y} and 1 runs



(f) Random tie breaking on \mathbf{y} and 20 runs



(g) Random noise tie breaking on \mathbf{y} and 1 run



(h) Random noise tie breaking on \mathbf{y} and 20 runs

Figure 8: Comparison of CCC values on tie breaking when both \mathbf{X} and \mathbf{y} have ties